Russian Geology and Geophysics © 2019, V.S. Sobolev IGM, Siberian Branch of the RAS
Vol. 60, No. 7, pp. 735–751, 2019 *DOI:10.15372/RGG2019049* *Geologiya i Geofizika*

Composition of Pyrrhotite as an Indicator of Gold Ore Formation Conditions at the Sovetskoe Deposit (Yenisei Ridge, Russia)

G.A. Palyanova [a,b,✉], A.M. Sazonov [c,d], T.V. Zhuravkova [a,b], S.A. Silyanov [c,d]

[a] *V.S. Sobolev Institute of Geology and Mineralogy, Siberian Branch of the Russian Academy of Sciences, pr. Akademika Koptyuga 3, Novosibirsk, 630090, Russia*

[b] *Novosibirsk State University, ul. Pirogova 1, Novosibirsk, 630090, Russia*

[c] *Siberian Federal University, Svobodnyi pr. 79, Krasnoyarsk 660041, Russia*

[d] *Tomsk State University, pr. Lenina 36, Tomsk, 634050, Russia*

Received 28 December 2017; received in revised form 1 June 2018; accepted 26 July 2018

Abstract—We present results of an investigation into the composition and parageneses of pyrrhotite at the Sovetskoe gold–quartz deposit (Yenisei Ridge, Russia). The variability of parameters (temperature T and sulfur fugacity f_{S_2}) during the stage crystallization of pyrrhotite-containing assemblages has been assessed from the composition of this mineral ($Fe_{0.873\pm0.02}S$–$Fe_{0.885\pm0.02}S$) and its parageneses. The compositions $Fe_{0.873–0.875}S$ close to Fe_7S_8 (Apy + Po + Rut + Qz), for which the estimated formation parameters are T = 486–465 ºC and $\log f_{S_2}$ = –4.71 to –5.28, are typical of early pyrrhotite in the form of microinclusions in arsenopyrite, associated with rutile and quartz. According to the composition of inclusions of pyrrhotite microcrystals ($Fe_{0.873–0.881}S$) associated with pyrite in native gold (950‰) (Au + Po + Py), the formation parameters are T = 489–410 ºC and $\log f_{S_2}$ = –4.63 to –6.98. Coarse pyrrhotite grains containing microinclusions of relict arsenopyrite and galena, sometimes, in aggregate with siderite (Po + Apy + Ga + Sid), and pyrrhotite in aggregate with pyrite and siderite (Py + Po + Sid) have composition $Fe_{0.874–0.878}S$ and form at 479–443 ºC and $\log f_{S_2}$ = –4.9 to –5.9. The xenomorphic pyrrhotite microinclusions present together with galena and native gold (950‰) in pyrite crystals (Py + Po + Ga + Au) are characterized by higher contents of iron ($Fe_{0.878–0.885}S$) and, correspondingly, lower temperatures of formation, 432–382 ºC, and $\log f_{S_2}$ = –6.27 to –7.95.

The $\log f_{S_2}$–T diagrams have been calculated for the systems Fe–S and Ag–Au–S in the temperature range 25–700 ºC with regard for the stability fields of iron sulfides (pyrite FeS_2, troilite FeS, and pyrrhotite Fe_7S_8), phases $Fe_{11}S_{12}$, $Fe_{10}S_{11}$, and Fe_9S_{10}, metallic iron, native sulfur, uytenbogaardtite, petrovskaite, and solid-solution phases $Fe_{1-x}S$ ($0 < x < 0.125$), $Ag_{1-z}Au_z$ (z = 0, 0.25, 0.5, and 1), and $Ag_{2-y}Au_yS$ (y = 0, 0.5, 1, and 2). The calculation results have demonstrated that there is a field of petrovskaite and uytenbogaardtite solid solutions and Au–Ag alloys (>670‰, $Ag_{0.5}Au_{0.5}$–Au) in the stability field of the pyrrhotite–pyrite parageneses of the Sovetskoe deposit. The gold and silver contents in iron sulfides of the Sovetskoe deposit show that the Au/Ag ratios in pyrrhotites (0.002–2.4) and pyrites (0.004–13) are lower than those in high fineness (950–980‰) gold (19–50). The difference in the Au/Ag ratios in these minerals and the results of thermodynamic calculations indicate the possible presence of Au–Ag sulfides and Au–Ag alloys of lower fineness in the pyrrhotite–pyrite ores of the studied deposit. The absence of visible mineral forms of gold sulfides from the ores suggests that these sulfides are present in finely dispersed or invisible microscopic forms. The pyrrhotite compositions in pyrite-containing parageneses as well as Au/Ag in pyrites, pyrrhotites, and visible native gold in sulfide ores of other gold and gold–silver deposits can be used to assess the possible presence of nanosized solid microinclusions of sulfide and other gold and silver forms.

Keywords: Sovetskoe quartz–gold deposit, pyrrhotite composition, pyrrhotite–(pyrite)-containing parageneses, acanthite, uytenbogaardtite, petrovskaite, nanosized microinclusions

INTRODUCTION

The composition of pyrrhotite and its mineral associations is an important information source about the physical and chemical conditions of their paragenesis. Modern ore-deposit formation models rely upon the physical and chemical conditions of mineralization and post-mineral transformation using such characteristics as temperature, pressure, sulfur (f_{S_2}) and oxygen (f_{O_2}) fugacity, pH and others (Barton and Toulmin, 1964; Holland, 1965; Kolonin et al., 1986; Kolonin and Palyanova, 1991; Bortnikov et al., 1996; Simon and Essene, 1996; Palyanova, 2008; Moloshag, 2009; Rottier et al., 2016). The sulfur fugacity is the most fundamental parameter when modeling sulfide ore genesis (Sack and Ebel, 2006 and their cited references). To obtain data about the temperature of mineral association formation, and sulfur fugacity one uses the mineral geothermometers based on different pyrrhotite–containing parageneses such as pyrrho-

✉ Corresponding author.
E-mail adress: palyan@igm.nsc.ru (G.A. Palyanova)

tite–pyrite, pyrite-pyrrhotite-magnetite, electrum-pyrite-pyrrhotite, pyrrhotite-arsenopyrite and others.

Pyrrhotite is an important sulfide mineral of magmatic (abyssal deposits related to basic and ultrabasic intrusive rocks) and, sometimes, of metamorphic, hydrothermal and diagenetic origin (Lennie and Vaughan, 1996; Gordon and McDonald, 2015). Its composition is nonstoichiometric, characterized by iron deficiency and high content of sulfur and describe by the formula $Fe_{1-x}S$ ($0 \le x \le 0.125$) or FeS_y ($1 \le y \le 1.143$). One extreme of this solid solution series (at $x = 0$ or $y = 1$) with composition FeS is known as troilite (of hexagonal syngony). The other extreme that can be written as $Fe_{0.875}S$ ($x = 0.125$), $FeS_{1.143}$ ($y = 1.143$), or as Fe_7S_8 is clinopyrrhotite (of monoclinic syngony) (Godovikov, 1983; Lennie and Vaughan, 1996). Low-temperature iron sulfides include greigite Fe_3S_4 ($Fe_{0.75}S$ or $FeS_{1.333}$), smythite $Fe_{11}S_{16}$ ($Fe_{0.6875}S$ or $FeS_{1.455}$), phases of composition—Fe_2S_3 ($Fe_{0.667}S$ or $FeS_{1.5}$), $Fe_{11}S_{12}$ ($Fe_{0.877}S$ or $FeS_{1.140}$), $Fe_{10}S_{11}$ ($Fe_{0.9}S$ or $FeS_{1.111}$) and Fe_9S_{10} ($Fe_{0.917}S$ or $FeS_{1.091}$) (Waldner and Pelton, 2005).

Being a nonstoichiometric mineral, pyrrhotite is used as an indicator of sulfur fugacity (Toulmin and Barton, 1964; Barton and Toulmin, 1964; Scott, 1976; Moloshag, 2009; Rottier et al., 2016), for its compositions often reflect the equilibrium condition during mineralization. Their capabilities for estimation of the temperature of pyrite-pyrrhotite association formation in nature have been demonstrated in (Arnold, 1962). The author has shown that a pressure below 2 kbar, as well as the presence of small amounts of nickel, cobalt, copper and manganese in its composition during pyrrhotite crystallization, has no effect on pyrrhotite composition. However, one of the main assumptions for utilizing this geothermometer has been that pyrite and pyrrhotite exist in equilibrium, and pyrrhotite composition does not change with passing geological time. The same author (Arnold, 1967) studied the compositions of natural pyrrhotites from 82 deposits worldwide. When in association with pyrites, these natural pyrrhotites are always iron depleted within the range from 46.5 to 47.5 at.% ($Fe_{0.869–0.905}S$) if compared to synthetic pyrrhotites, which limits using this geothermometer in the low-temperature domain.

A number of authors (Skornyakov, 1947; Sazonov et al., 1992; Craig and Vokes, 1993; Tyukova and Voroshin, 2007) described pyrrhotite pseudomorphs that developed from pyrites and seemed to mark a metamorphic boundary, above which pyrite decomposed and pyrrhotite formed. Many massive sulfides contain sufficient amounts of coexisting pyrite and pyrrhotite that are interpreted as primary phases (Craig and Vokes, 1993).

The presented study describes the pyrrhotites from the Sovetskoe deposit (Yenisei Ridge, Russia) classified as one of low-sulfide gold–quartz type that are found graphite-bearing black shales (Smirnov, 1978; Sazonov et al., 1991; Rusinova et al., 1999; Tomilenko and Gibsher, 2001; Silyanov and Nekrasova, 2015).

The objective of the study was to investigate the compositions of the pyrrhotites and their associated minerals based on temperature and sulfur fugacity (f_{S_2}) changes and to determine the stability conditions for iron sulfides, and natural Au–Ag alloys and Au–Ag sulfides as acanthite, uytenbogaardtite and petrovskaite. Since Au–Ag sulfides are difficult to detect and are often found as microinclusions in pyrite and non-ferrous sulfide ores, their presence can be assumed through physical and chemical modeling of sulfide systems. The possible indicators of such inclusions may be pyrrhotite compositions and their mineral associations as well as the Au/Ag ratios in iron sulfides (pyrite, pyrrhotite) and native gold.

OBJECT AND METHODS OF RESEARCH

The object of the presented research is the sulfide ores of the Northwestern quarry of the Sovetskoe deposit (Krasnoyarsk region, Russia) impregnated with pyrrhotite, pyrite, arsenopyrite, native gold and other minerals. The quarry has stripped ore zones I–IV in the near-surface part of the deposit, where ore remining takes place. This part of the deposit was initially developed in the 1950s. At that time, the richest parts of the ore bodies were mined. Current production concerns the ores that have been outlined according to present day quality requirements. The Sovetskoe deposit is placed in the northeastern part of the Yenisei Ridge (Fig. 1) and takes utmost northwestern potion in the submeridionally extended gold ore belt of the Eastern gold-bearing belt of the Yenisei Ridge. For about 100 years of gold mining, the deposit has produced about 90 tons of noble metals, the first hundreds of kilograms—in the years before the Revolution. According to regional forecast metallogenic studies, the deposit has not yet been depleted and its reserves are concentrated in its deep horizons. In the 1980s, the exploration wells of Yenisei Gold (Yeniseizoloto) detected commercial gold mineralization within the interval of 250–600 m, below a quartz vein zone already being mined. Underground mining at the deposit was stopped at the beginning of the 1990s while quarry mining continued until 2016.

The deposit's ore bodies are composed of quartz (up to 80 wt.%), enveloping shale relicts and sulfides whose amount does not exceed 5 wt.%. The basic ore minerals are pyrite and pyrrhotite that are mainly monoclinic (magnetic) but hexagonal pyrrhotite (nonmagnetic) and arsenopyrite present as well. Other minor minerals are galena, sphalerite, chalcopyrite and native gold. Rare ones include bismuthinite, native silver and freibergite.

Figure 2 demonstrates photos of ore samples from the Sovetskoe deposit that have been found in the Northwestern quarry in a site of 1×3 m^2 in size. The site had a fragment of an ore body being a quartz vein with sulfide pockets and visible gold impregnations. The samples are milky-white pyrite-quartz and pyrrhotite-quartz aggregates (Fig. 2*b*, *c*)

with shale relicts (Fig. 2*a*). The visible native gold is located in the quartz fractures (Fig. 2*a*).

The deposit has undergone two ore-deposition stages. Its early productive stage was the formation of sequential and morphologically complex quartz-vein bodies grouping into zones. The mineral associations of the first productive stage included large amounts of ilmenite, rutile, sphene, zircon, monazite, graphite, apatite, tourmaline, magnetite, chlorite, muscovite and albite. These minerals are the relict substance of the enveloping phyllonites that underwent assimilation and recrystallization in the quartz-vein mass. At this stage, grain sizes of native gold were microscopic and presented themselves as microinclusions in early sulfides and nonmetallic minerals.

The late productive stage started after a long break and decomposition of the quartz-sulfide material that had formed earlier (Petrovskaya, 1954). The mineral associations of this gold–sulfide–polymetallic stage developed in the fractures propagating in the submeridional and northwestern directions and include veins and pockets of siderite, ankerite, and seemingly macroscopic aggregates of pyrite, pyrrhotite, chalcopyrite, sphalerite, galena and native gold. The microscopic aggregates, apart from sulfides, include bismuthine antimony and silver-antimony fahlores, native silver, calaverite and other tellurides (Petrovskaya, 1954). The second-stage mineral aggregates are impregnated into the bulk of first-stage minerals that form the telescoped ores of the first and second stages of ore genesis. The ore microstructures also demonstrate typical zonal distribution of early and late minerals (Fig. 3). Thus, the early sulfide minerals are separated from the late pyrites with an ankerite–sphalerite band, and the sphalerite association often includes chalcopyrite. The early pyrite is corroded by pyrrhotite and is often replaced to the degree of complete pseudomorphs. The galena is usually microscopically impregnated and does not aggregate with any other minerals. It is distributed uniformly in the sphalerite–chalcopyrite aggregates, carbonates and quartz. The native gold often aggregates with minerals of sulfide–polymetallic stage, forming inclusions in them. Like galena, the native gold has no tight spatial connection with the sulfides. More often than not, these inclusions are monomineral aggregates filling the intergrain space and cataclastic fractures in the quartz.

After a microscopic study, the selected ore samples underwent soft crushing to separate monomineral fractions of pyrite, pyrrhotite and native gold to be studied using an Olympus BX51 optic microscope. The investigation methods included scanning electron microscopy, electron microprobe analysis (EPMA) and X-ray powder diffraction (XRD). The chemical composition of pyrite, pyrrhotite, native gold and other minerals was studied using such scanning electron microscopes as MIRA 3 LMU (TESCAN Ltd.) with an INCA Energy 450+ energy dispersive spectrometer (Analytical Center for Multielemental and Isotope Research SB RAS, Novosibirsk, Russia, analyst N.S. Karmanov) and a VEGA II LMU with an OXFORD INCA ENERGY 350 integrated X-ray energy dispersive microanalyzer (Analytic Center for Natural Systems Geochemistry, Tomsk State University, Tomsk, Russia, analyst E.V. Korbovyak).

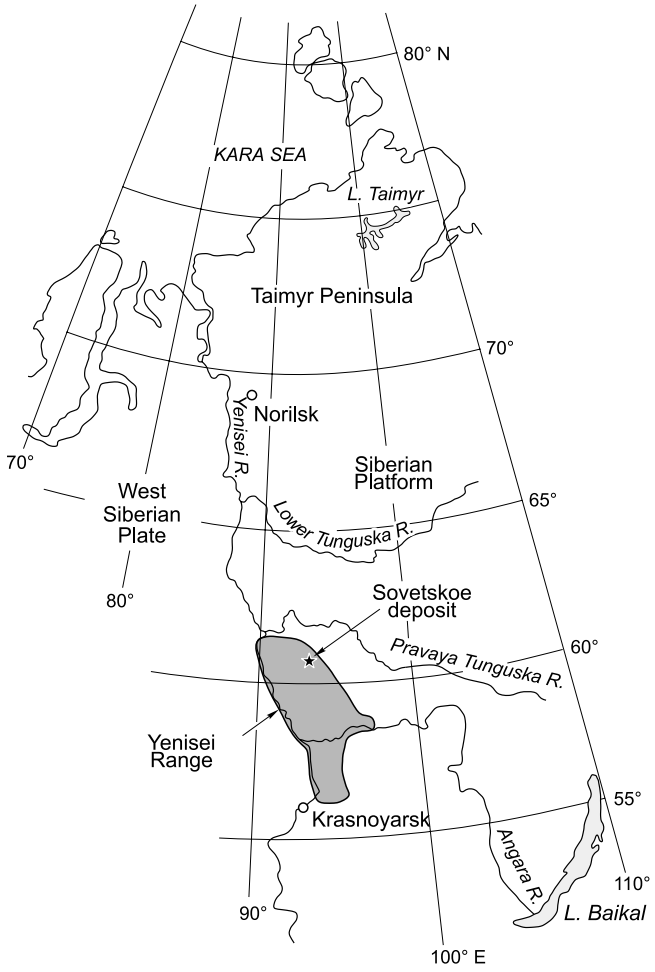

Fig. 1. Geological and geographical location of the Sovetskoe deposit.

During the scanning microscopy investigation, the spectrum accumulation time comprised either 15–20 or 70–100 s. The analyzed grains' size was 5 μm and more in order to avoid the background elements presented in the surrounding phases. As ore-element references, we used Ag, Au–Ag alloys, Au, Cu, FeS_2 and PbS. The detection limits for the ore elements were tenths of a percent, and the error rate for the main components (> 10–15 wt.%) did not exceed 1 rel.%, and for the components with the concentration of 1–10 wt.%—< 2 rel.%. Table 1 demonstrates the extreme values of pyrrhotite for each mineral association that we obtained from EPMA of a typical grain in 5–10 points.

The sample gold and silver contents were detected using the ICP-MS method with an Agilent 7500cx mass spectrometer (Agilent Technologies). Before the study, using the incremental decomposition technique the weighted sulfide probes were converted into solutions of nitric and nitrohydrochloric acids to keep in fluid phase and analyze gold,

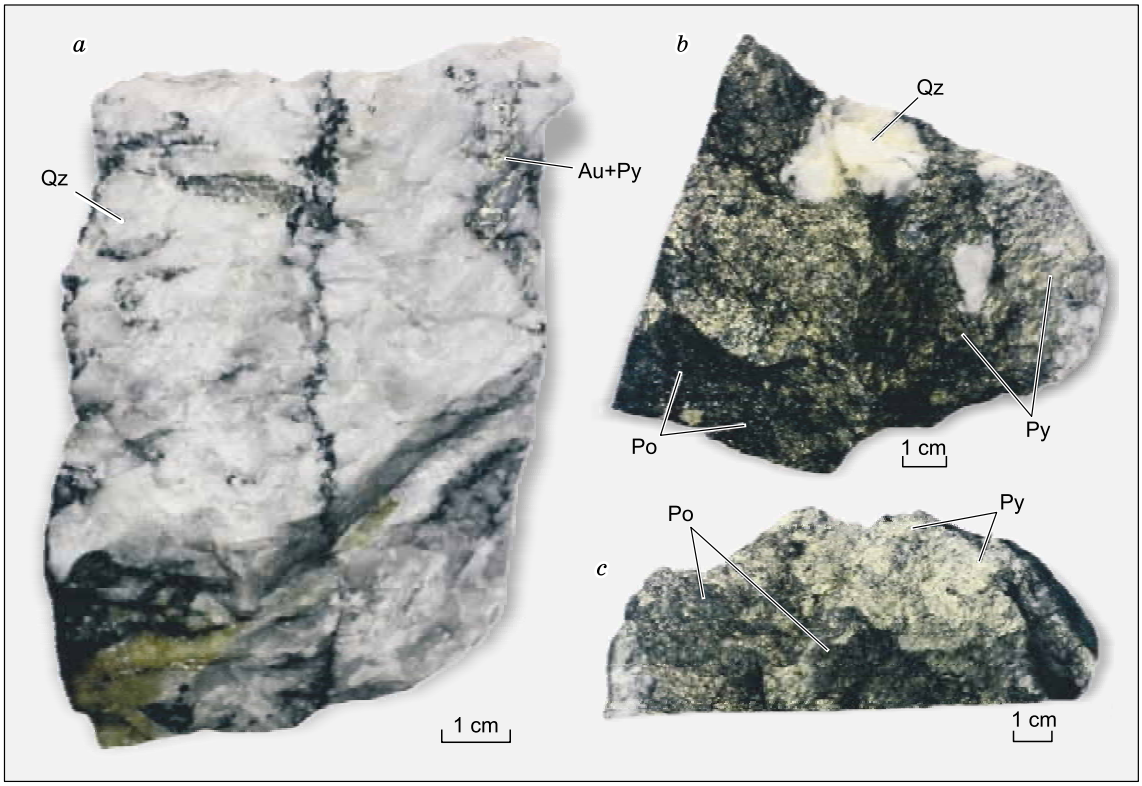

Fig. 2. Ore samples macrophotographs: *a*, sample 2-1/28, milky-white quartz with shale relicts, pyrites and native gold in fractures; *b*, sample 2-22, brecciated quartz with a cemented confluent pyrite-pyrrhotite aggregate (with a tarnish); *c*, sample 2-20, confluent pyrite-pyrrhotite aggregate with quartz chippings.

silver and other elements. The quality of the obtained measurements was estimated based on the BCR-2, BHWO, SSL-1 and other standards. The analyses were performed in the Analytic Center for Natural Systems Geochemistry, Tomsk State University, Tomsk (analysts E.V. Rabtsevich and E.I. Nikitina).

The Au and Ag contents in the pyrites and pyrrhotites of ore zone VI were determined through atomic absorption analysis (analyst V.G. Tsimbalist, V.S. Sobolev Institute of Geology and Mineralogy, Siberian Branch of the Russian Academy of Sciences).

The concentrations of gold, silver and other microinclusions in the iron sulfides were measured using the LA-ICP-MS method with an XSeries quadrupole mass spectrometer equipped with a NewWave UP-213 laser sampler. The sampling was performed at the laser's frequency of 15–20 Hz, beam diameter of 40–60 μm and energy density 7–10 J/cm^2 (Institute of Ore Deposits Geology, Petrography, Mineralogy and Geochemistry, RAS, Moscow, analyst V.D. Abramova). The pyrite and pyrrhotite grains were penetrated using point-by-point and profile (groove) ablation. The profile scanning rate was 5 μm/s. The duration of a point measurement was 60 s. For most of the elements, the sensitivity varied from 0.02 to 0.05 ppm. For sulfide analysis, we relied on two standards: MASS1 (USGS), pressed granules of synthetic polymetallic sulfide ZnCuFeS; and po-stc containing 20 ppm of Au, Ag and PGE in a pyrrhotite matrix produced as described in (Ballhaus et al., 2006). The obtained data were calculated using the Iolite application for the IgorPro package (Paton et al., 2011).

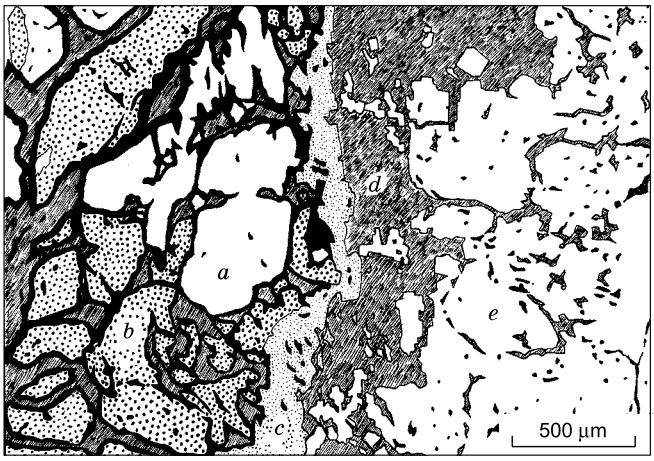

Fig. 3. Zonal distribution of early and late sulfides in ores. *a*, Pyrite-I, *b*, pyrrhotite, *c*, sphalerite-chalcopyrite aggregate, *d*, ankerite, *e*, pyrite-II. The sketch of ore aggregate was drawn by A.S. Kotelnikov.

Table 1. Pyrrhotite composition and its mineral associations in the Sovetskoe deposit; estimated crystallization temperatures and sulfur fugacity values

Sample No.	S wt.%	Fe	Σ	S at.%	Fe	$Fe_{1-x}S$	FeS_y	*T*, °C	$\log f_{S_2}$ (1/2)**	Mineral associations	m.a. No.
Pyrrhotite microinclusions in native gold, pyrite and arsenopyrite											
2-1/28	39.27	59.71	98.98	53.39	46.61	$Fe_{0.873}S$	$FeS_{1.145}$	485.9	–4.71/–4.71	Apy + Po + Rut + Qz (Fig. 8*a*)	1
2-1/28	39.02	59.5	98.52	53.32	46.67	$Fe_{0.875}S$	$FeS_{1.142}$	465.4	–5.21/–5.28	Pyrrhotite, rutile and quartz inclusions in arsenopyrite	
						$Fe_{0.873-0.875}S$	$FeS_{1.145–1.142}$	486–465	–4.71 ÷ –5.28	Apy + Po + Rut + Qz	1
2-1/28	39.77	60.69	100.46	53.3	46.7	$Fe_{0.876}S$	$FeS_{1.141}$	457.4	–5.42/–5.51	$Au_{(950)}$ + Po (Fig. 4)	2a
2-1/28	39.46	60.59	100.05	53.15	46.85	$Fe_{0.881}S$	$FeS_{1.134}$	410.1	–6.73/–6.98	Pyrrhotite inclusions in native gold	
2-1/28	39.68	60.33	100.01	53.4	46.6	$Fe_{0.873}S$	$FeS_{1.146}$	489.1	–4.64/–4.63	$Au_{(950)}$ + Po + Py (Fig. 5)	2b
2-1/28	39.44	60.08	99.52	53.35	46.65	$Fe_{0.874}S$	$FeS_{1.144}$	473.2	–5.02/–5.06	Pyrrhotite and pyrite inclusions in native gold	
						$Fe_{0.873–0.881}S$	$FeS_{1.146–1.134}$	489–410	–4.63 ÷ –6.98	$Au_{(950)}$ + Po + Py	2
2-1/28	39.46	60.42	99.88	53.22	46.78	$Fe_{0.878}S$	$FeS_{1.138}$	432.1	–6.09/–6.27	Py + Po + Ga + Au (Figs. 6, 7)	5
2-1/28	39.11	60.28	99.39	53.06	46.94	$Fe_{0.885}S$	$FeS_{1.130}$	381.9	–7.60/–7.95	Pyrrhotite, galena and native gold inclusions in pyrite	
						$Fe_{0.878-0.885}S$	$FeS_{1.138-1.130}$	432-382	–6.27 ÷ –7.95	Py + Po + Ga + Au	5
Coarse pyrrhotite grains in aggregation with arsenopyrite, galena, pyrite and siderite											
2-22_4	38.75	58.99	97.74*	53.37	46.63	$Fe_{0.874}S$	$FeS_{1.144}$	479.0	–4.88/–4.90	Po + Apy + Ga + Sid (Fig. 8*b*)	3
2-22_3	38.70	59.18	97.88*	53.25	46.75	$Fe_{0.878}S$	$FeS_{1.139}$	442.8	–5.80/–5.94	Pyrrhotite with arsenopyrite and galena inclusions (in aggregation with siderite)	
						$Fe_{0.874–0.878}S$	$FeS_{1.144–1.139}$	479–443	–4.88 ÷ –5.94	Po + Apy + Ga + Sid	3
2-20	38.89	59.3	98.19*	53.32	46.68	$Fe_{0.875}S$	$FeS_{1.142}$	464.8	–5.23/–5.30	Py + Po + Sid (Fig. 8*c*)	4
2-22-6	38.61	58.94	97.55*	53.30	46.70	$Fe_{0.876}S$	$FeS_{1.141}$	457.4	–5.42/–5.51	Pyrrhotite in aggregation with pyrite and siderite	
						$Fe_{0.875–0.876}S$	$FeS_{1.142–1.141}$	465–457	–5.23 ÷ –5.51	Py + Po + Sid	4

Note. m.a. No., Means the serial numbers of mineral associations with the pyrrhotites of different composition and/or pyrite (Figs. 10, 11).
* Analyses were performed in the Analytical Center for Natural Systems Geochemistry, Tomsk State University, Tomsk, analyst E.V. Korbovyak, the others are the data provided by the Analytical Center for Multielemental and Isotope Research, SB RAS, Novosibirsk (analyst N.S. Karmanov).
**1, from (Toulmin and Barton, 1964); 2, from (Osadchii and Chareev, 2006).

RESULTS

EPMA results. The studied fragments of pyrrhotite-bearing ores have differences both in their chemical composition and in the way the pyrrhotite relates to its neighboring minerals (Figs. 4–8). The results of EPMA for different pyrrhotite associations can be seen in Table 1. For the sake of convenience, the pyrrhotite compositions are given both in atomic and weight percent. Further in the text, we use at.% and the formula units of $Fe_{1-x}S$ to characterize pyrrhotite compositions from different mineral associations.

Pyrrhotite often occurs as microinclusions in other minerals such as pyrite, arsenopyrite and native gold (Figs. 4–7, 8*a*). The larger accumulations of this mineral aggregate with pyrite, arsenopyrite and siderite (Fig. 8*b*, *c*).

The early-stage pyrrhotite occurring together with rutile and quartz as microinclusions in arsenopyrite (Fig. 8*a*) is characterized by narrow intervals of iron (46.61–46.67 at.%) and sulfur (53.39–53.30 at.% ($Fe_{0.873–0.875}S$)) concentration variations (Table 1, mineral association 1: Apy + Po + Rut + Qz). Their composition is close to the extreme one of pyrrhotite solid solutions Fe_7S_8 ($x = 0.875$). The composition of the arsenopyrite matrix is characterized by iron deficiency and sulfur prevalence over arsenic: $Fe_{0.971}As_{0.972}S_{1.028}$.

The microinclusions (20–70 μm in size) of hexagonal pyrrhotite are often present in the coarse grains of native gold (100–500 μm) (Figs. 4, 5). Apart from pyrrhotite, native gold often contains pyrite (Fig. 5). The pyrrhotite-native gold associations has iron quantities varying from 46.6 to 46.85 at.% and sulfur from 53.4 to 53.15 at.% ($Fe_{0.873–0.881}S$) (Table 1, mineral association 2: Au + Po + Py). EPMA of the native gold aggregated with pyrrhotite and pyrite shows the presence of silver (5 wt.%), which corresponds to a high fineness of 950‰, $Au_{0.91}Ag_{0.09}$.

Coarse pyrrhotite grains with microinclusions of arsenopyrite or galena or both of them (Fig. 8*b*) in association with siderite are characterized by iron content varying from 46.63 to 46.75 at.% and sulfur from 53.37 to 53.5 at.%, $Fe_{0.874–0.878}S$ (Table 1, mineral association 3: Po + Apy + Ga + Sid). Arsenopyrite composition is close to the stochiometric

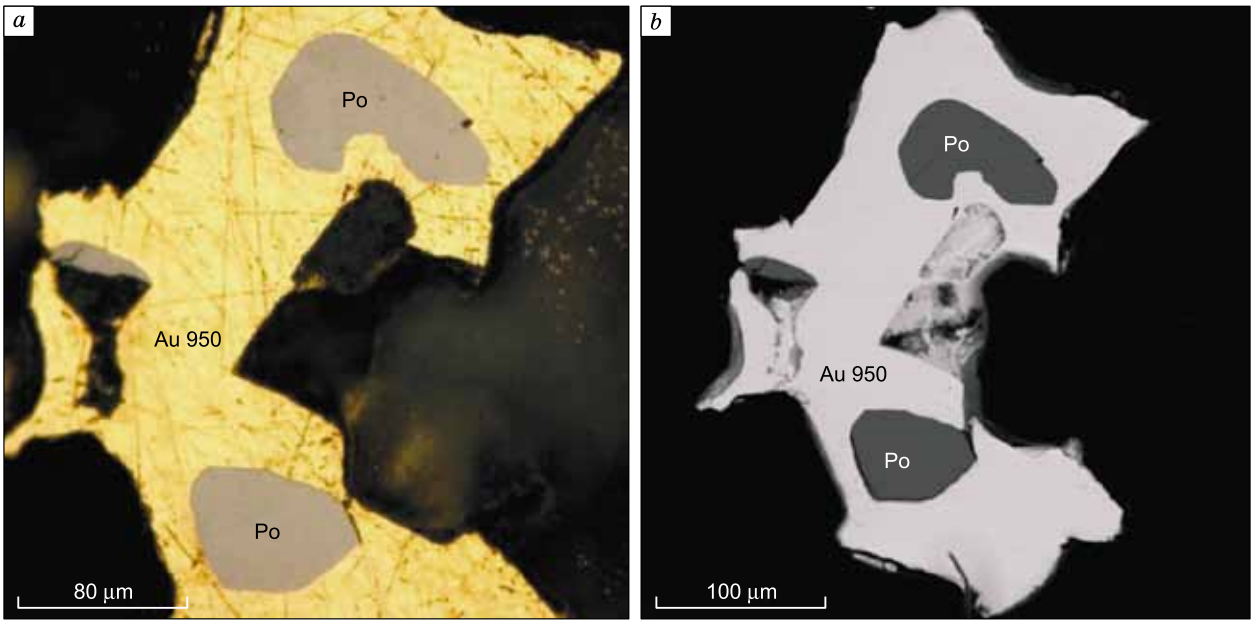

Fig. 4. Optic (*a*) and SEM (*b*) photos of high fineness gold (Au, fineness 950 ‰) with inclusions of hexagonal pyrrhotite (Po, $Fe_{0.873–0.881}S$).

one with insignificant prevalence of sulfur over arsenic and cobalt impurities, which does not entirely compensate the iron deficit: $(Fe_{0.885}Co_{0.089})_{0.974}As_{0.993}S_{1.007}$.

When aggregated with pyrite and siderite, pyrrhotite (Fig. 8*c*) has a stable composition with low iron (46.68–46.70 at.%) and high sulfur (53.32–53.30 at.%) concentrations, $Fe_{0.875–0.876}S$ (Table 1, mineral association 4: Po + Py + Sid).

The xenomorphic inclusions of pyrrhotite, galena (Fig. 6) and native gold (fineness 950‰, Fig. 7) are often found in pyrite crystals. The amount of iron in such pyrrhotite inclusions varies from 46.78 to 46.94 at.% and that of sulfur from 53.22 to 53.06 at.%, $Fe_{0.878–0.885}S$ (Table 1, mineral association 5: Py + Po + Ga + Au). Galena and pyrite have stochiometric compositions.

Thus, the iron and sulfur variations in the studied pyrrhotite samples embrace the intervals from 46.6 to 46.94 at.% Fe and from 53.4 to 53.06 at.% S ($Fe_{0.873–0.885}S$) and depend on an association mineral composition.

LA-ICP-MS results for pyrrhotite and pyrite. LA-ICP-MS and atomic absorption analysis were used to detect the concentrations of gold, silver and other microinclusions in the pyrrhotites and pyrites of the Northwestern quarry and ore zone VI of the Sovetskoe deposit.

The concentration of invisible silver in the pyrrhotite of mineral association Py + Po + Sid reaches 0.06–0.41 ppm and that of gold <0.02 ppm (in most cases below the sensitivity range) (Table 2). The pyrrhotite also contains impurities (in ppm) of Cr (up to 2760), Co (up to 111), Ni (up to 960), Cu (up to 216), Zn (up to 420), Pb (up to 2.2) and As

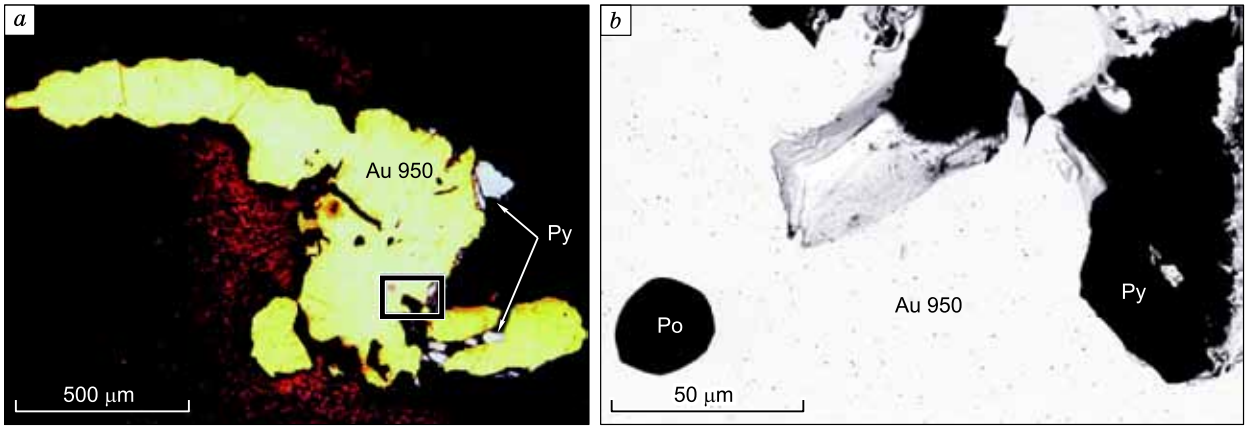

Fig. 5. *a*, Optic photos, high fineness gold (Au, fineness 950‰) with pyrite (Py) and hexagonal pyrrhotite (Po, $Fe_{0.873–0.874}S$) inclusions; *b*, SEM photo, zoomed fragment of Fig. 5*a* marked with black contour.

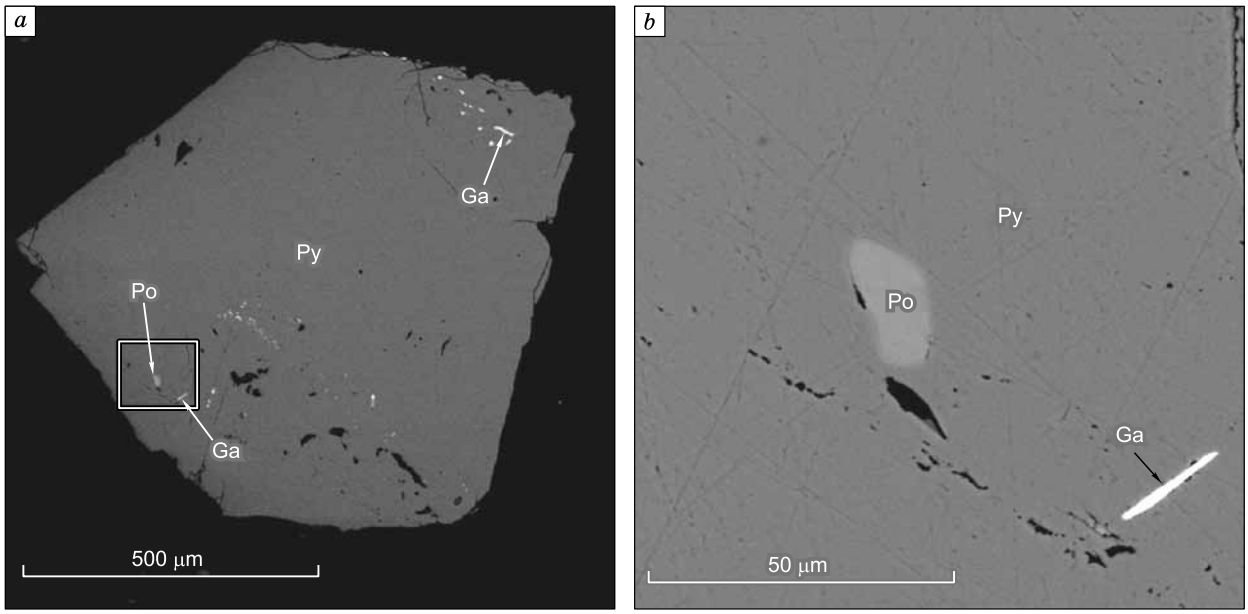

Fig. 6. SEM photo of pyrite (Py) with pyrrhotite (Po, $Fe_{0.878–0.885}S$) and galena inclusions.

(up to 71). In some zonal grains As concentration increases from the center to the margins from 26 to 50 ppm but it has no correlation with any other elements.

The pyrites of mineral associations Py + Po + Ga + Au and Py + Po + Sid have a similar set of microinclusions (Cr, Co, Ni, Co, Cu, Zn, Pb, As, Au and Ag, Fig. 9), while the concentrations of other detected elements (Se, Cd, Sb, Te, Hg, PGE) are below the sensitivity range. The pyrites of mineral association Py + Po + Ga + Au could be divided into those associated with "invisible" (Py-2) and visible (Py_{Au}-2) gold. The Py-2 pyrites contain impurities (in ppm) of Cr (up to 6), Co (up to 7.8), Ni (up to 380), Cu (up to 10.2), As (up to 2175), Pb (up to 3) and Bi (up to 0.5). Their gold content varies from 0.1 to 0.4 ppm, and that of silver—below the sensitivity range. The Py_{Au}-2 pyrites have higher gold (1.4 ÷ 7.6 ppm) and silver (0.3 ÷ 0.7 ppm) concentrations, which corresponds to Au/Ag ratios of 4.0–13.6. The amounts of Cr, Co and Ni are also higher than those in the pyrites with invisible gold and reach 40, 150 and 806 ppm respectively. For the pyrites of Py + Po + Sid the following concentrations of impurities (in ppm) were detected: Cr (up to 1140), Co (up to 137), Ni (up to 1350), Cu (up to 38), Zn (up to 49), Pb (up to 2.3), As (up to 28.6), Ag (up to 0.13), Au—below the sensitivity range.

Method of estimation of temperatures and sulfur fugacity. According to the Fe–S phase diagram in Fig. 10, within the temperature range of 250–743 °C a pyrite–pyrrhotite association that has formed as:

$$FeS_2 = FeS_y + 0.5(2 - y)\ S_{2(g)} \quad (1)$$

should be considered stable. However, the y variations are limited to $1 < y < 1.23$. Below is an equation that binds pyrrhotite composition in equilibrium with pyrite as the function of temperature calculated for this reaction in (Lambert et al., 1998):

$$y = 4.3739\cdot10^{-12}\cdot T^4 - 1.2034\cdot10^{-8}\cdot T^3 + 1.2365\cdot10^{-5}\cdot T^2 - 5.4779\cdot10^{-3}\cdot T + 1.99, \quad (2)$$

where T is the temperature from 523 to 1016 K (or 250–743 °C), and y is the excessive molar fraction of S in relation to Fe at $1 < y < 1.23$.

Since the y-temperature dependence is linear, for the interval from 523 to 820 K (250–547 °C), it is determined by a simple equation:

$$y \text{ in } FeS_y = 1.45\cdot10^{-4}\cdot T(\text{K}) + 1.0354, \quad (3a)$$

so, the temperature can be calculated either from the derived equation below:

$$T(\text{K}) = (y - 1.0354)/0.000145 \quad (3b)$$

or estimated by trial and error.

The formulas describing sulfur fugacity dependence on temperature in nonstoichiometric pyrrhotite have been published in numerous works (Toulmin and Barton, 1964; Osadchii and Chareev, 2006; Wang et al., 2006; Chareev et al., 2014). In (Wang et al., 2006) the authors derive an equation to calculate sulfur fugacity and temperature for $Fe_{1-x}S$ ($0 < x < 0.125$) pyrrhotites, which can also be used to estimate sulfur fugacity in two-phase system $Fe_{1-x}S–S_{2(g)}$.

In (Toulmin and Barton, 1964) the authors derive the equation for pyrite–pyrrhotite buffer:

$$\log f_{S_2} = (70.03 - 85.83\cdot N)\cdot(1000/T - 1) + 39.3\cdot\sqrt{(1 - 0.9981\cdot N)} - 11.91 \ (325 \le T, ^\circ\text{C} \le 743), \quad (4)$$

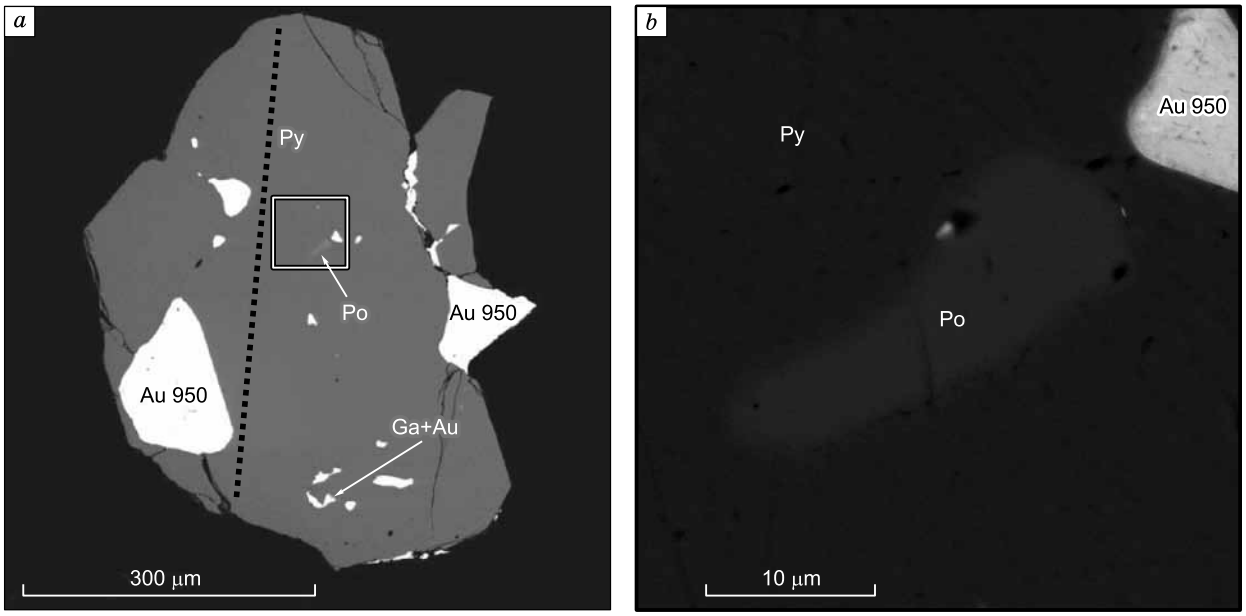

Fig. 7. SEM photo of pyrite (Py) with pyrrhotite (Po, $Fe_{0.878–0.885}S$), native gold (Au, fineness 950‰) and galena (Ga) inclusions.

where N denotes the molar fraction of S in pyrrhotite FeS_N in the system FeS–S_2, where $N = 2/(1 + y)$.

In (Osadchii and Chareev, 2006) the authors, using the method of solid galvanic cell to determine sulfur fugacity dependence on temperature at equilibrium line γ-Po (Fe_7S_8) + Py obtain the equation ascertaining the one published in (Toulmin and Barton, 1964):

$$\log f_{S_2} = 15.64 - 15455/T + \exp(10.2 - 11280/T)$$

$$(601 < T, \text{K} < 1016)\ (327 \le T, ^\circ\text{C} \le 743) \qquad (5)$$

In the presented study, equations (4) and (5) were used to estimate f_{S_2} in the temperature interval of 327–700 °C. For lower temperatures $\log f_{S_2}$ could be estimated using the formula from (Chareev and Osadchii, 2005):

$$\log f_{S_2}\ (\beta\text{-Po}, \alpha\text{-Po} + \text{Py}) = 39.76 - 29305/T$$

$$(298.15 \le T,\ \text{K} \le 565)\ (25 \le T, ^\circ\text{C} \le 292) \qquad (6)$$

Based on the data for pyrrhotite formation temperatures obtained from either equation (1) or (3a), sulfur fugacity values ($\log f_{S_2}$) were calculated from equations (4–6). In (Shi, 1992) the author demonstrates that the pressure up to 2 kbar has almost no effect on sulfur fugacity.

The results of the estimation of physicochemical parameters. Table 1 shows the temperature and sulfur fugacity intervals calculated from the equations presented above. Note that the sulfur fugacity values obtained from the equations in (Toulmin and Barton, 1964; Osadchii and Chareev, 2006; Chareev et al., 2014) are very close (Table 1). The sulfur fugacity data calculated using the equations from (Osadchii and Chareev, 2006; Chareev et al., 2014) ascertaining the data from (Toulmin and Barton, 1964) have been used further in the text to compare $\log f_{S_2}$ for different mineral associations.

For the microinclusions of $Fe_{0.873–0.875}S$ pyrrhotite, rutile and quartz in arsenopyrite (mineral association 1: Apy + Po + Rut + Qz), the estimated temperature and sulfur fugacity intervals were 486–465 ºC and from –4.71 to –5.28, respectively (Table 1, Figs. 10, 11). For the arsenopyrite matrix, these parameters estimated using Kretschmar and Scott's geothermometer (Kretschmar and Scott, 1976) changed from 460 to 300 °C, and from –5.0 to –14.6, respectively.

For pyrrhotite ($Fe_{0.873–0.881}S$) forming microcrystals of hexagonal habit in high fineness gold (950‰) (mineral association 2: Au + Po + Py) the obtained temperature and sulfur fugacity intervals were 489–410 °C and from –4.63 to –6.98, respectively (Table 1, Figs. 10, 11).

In the coarse pyrrhotite grains ($Fe_{0.874–0.878}S$) with microinclusions of arsenopyrite and/or galena in aggregate with siderite (mineral association 3: Po + Apy + Ga + Sid) as well as pyrrhotite ($Fe_{0.875–0.876}S$) in aggregates with pyrite and siderite (mineral association 4: Py + Po + Sid) the estimated crystallization temperature and sulfur fugacity intervals are 479–443 °C and from –4.9 to –5.9, respectively (Table 1, Figs. 10, 11).

The pyrrhotite ($Fe_{0.878–0.885}S$) forming xenomorphic microinclusions together with galena and high fineness gold (950‰) in pyrite crystals that had higher iron contents (mineral association 5: Py + Po + Ga + Au) is characterized by lower temperature and sulfur fugacity intervals to be 432–382 °C and from –6.27 to –7.95, respectively.

The results of electron probe microanalysis of the composition of the pyrrhotites being a part of different mineral associations found in the Sovetskoe deposit have demonstrated that their content of ore-forming elements varies

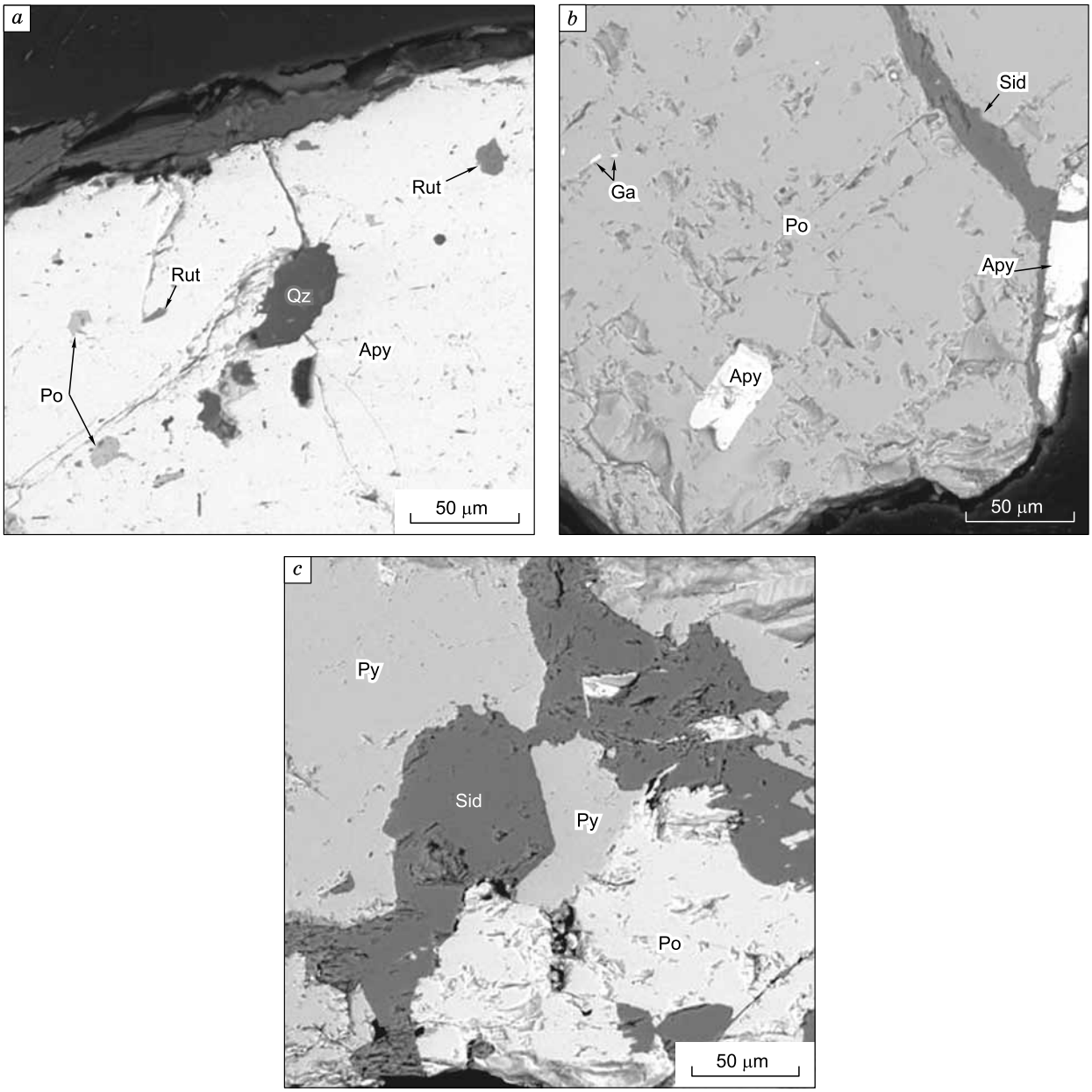

Fig. 8. SEM photo of pyrrhotites (Po) in association with arsenopyrite, galena, pyrite and siderite. *a*, Pyrrhotite ($Fe_{0.873–0.875}S$), rutile and quartz inclusions in arsenopyrite, *b*, pyrrhotite ($Fe_{0.874–0.878}S$) with inclusions of arsenopyrite, galena, and siderite veinlets, *c*, pyrrhotite ($Fe_{0.875–0.876}S$) in aggregation with pyrite and siderite.

within the intervals (at.%) from 46.6 to 46.94 for Fe and from 53.4 to 53.06 for S, which in formula units $Fe_{1-x}S$ equals to $Fe_{0.873±0.002}S$ to $Fe_{0.885±0.002}S$ (Table 1). In accord with these extreme pyrrhotite compositions, their maximum crystallization temperature for pyrrhotites with minimum iron content will be 489 °C, and with maximum iron content—382 °C. The maximum and minimum sulfur fugacity values will be –4.63 and –7.95, respectively. According to experimental results (Arnold, 1962), the temperature interval for pyrrhotite formation in the Sovetskoe deposit corresponds to ≈490–390 °C.

The obtained results for pyrrhotite compositions and sulfide crystallization temperatures lie within the temperature interval of quartz vein formation, which was determined for the deposit using thermobarogeochemical methods (Tomilenko and Gibsher, 2001). According to the authors the quartz vein zones of the deposit were formed during regional greenschist metamorphism at temperatures 100–410 °C and pressures 0.5–1.5 kbar by mostly homogenous solutions, whose salinity was below 8 wt.% of NaCl-equiv, and CO_2 content from 2.7 to 7.5 mol.%. Quartz vein ore zones, one the other hand, were formed due to later geother-

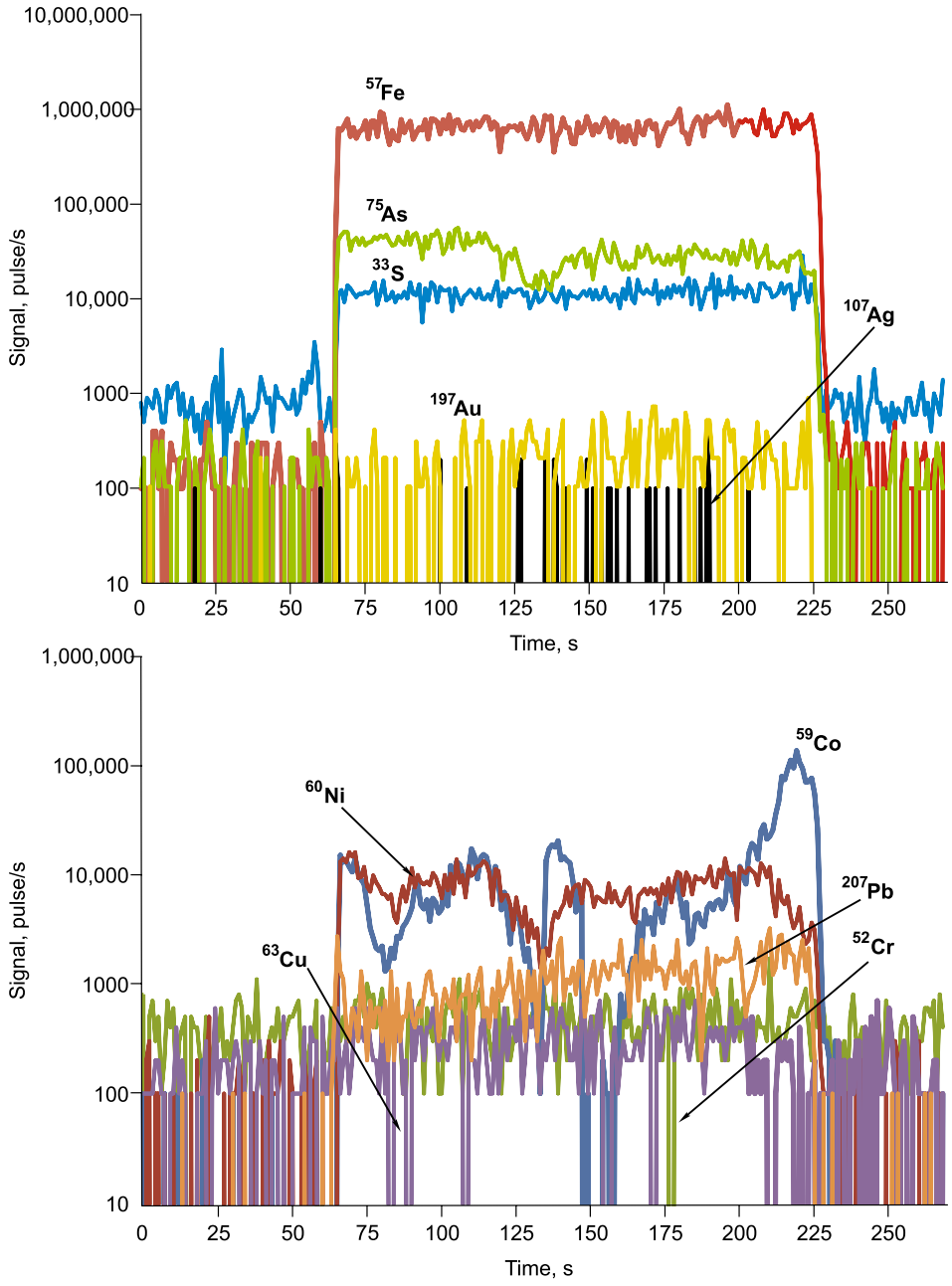

Fig. 9. LA-ICP-MS element concentration spectra for the pyrite of the 2nd mineral association. Profile positioning can be seen in Fig. 7*a*. The vertical axis denotes the number of impulses per second, the horizontal one—timeline.

mal activity at the temperatures of 100–630 °C, the pressure of 0.7–2.0 kbar by both homogeneous and heterogeneous solutions, whose salinity reached 20–25 wt.% of NaCl-eqv., CO_2 content—62.0 mol.%, CH_4—3.0 mol.%, N_2—13.2 mol.%. Thus, the total ore-forming interval lies within the temperature range of 100–630 °C at the pressure below 2 kbar, which been confirmed by both thermobarogeochemical data and our own.

Phase equilibria in the Fe–Ag–Au–S system (thermodynamic calculations). The phase equilibria for two systems (Fe–S and Ag–Au–S) and the temperature range of 25–700 °C can be seen in Fig. 11 (log f_{S_2}–T diagram). If compared to the Fe–S diagram for temperature range of 250–850 °C published earlier in (Toulmin and Barton, 1964), the presented one has been extended to 25 °C and corrected to account the refined thermodynamic constants for iron sulfides. According to the data that were published later for the same system (Gronvold and Stolen, 1992; Lambert et al., 1998; Waldner and Pelton, 2005), at the temperature range below 320 ºC, 5 phases remain stable, and these are FeS, Fe_7S_8, $Fe_{11}S_{12}$, $Fe_{10}S_{11}$ and Fe_9S_{10}. Estimations of their thermodynamic functions, as well as those for other phases of Fe–S, have been given in (Waldner and Pelton, 2005).

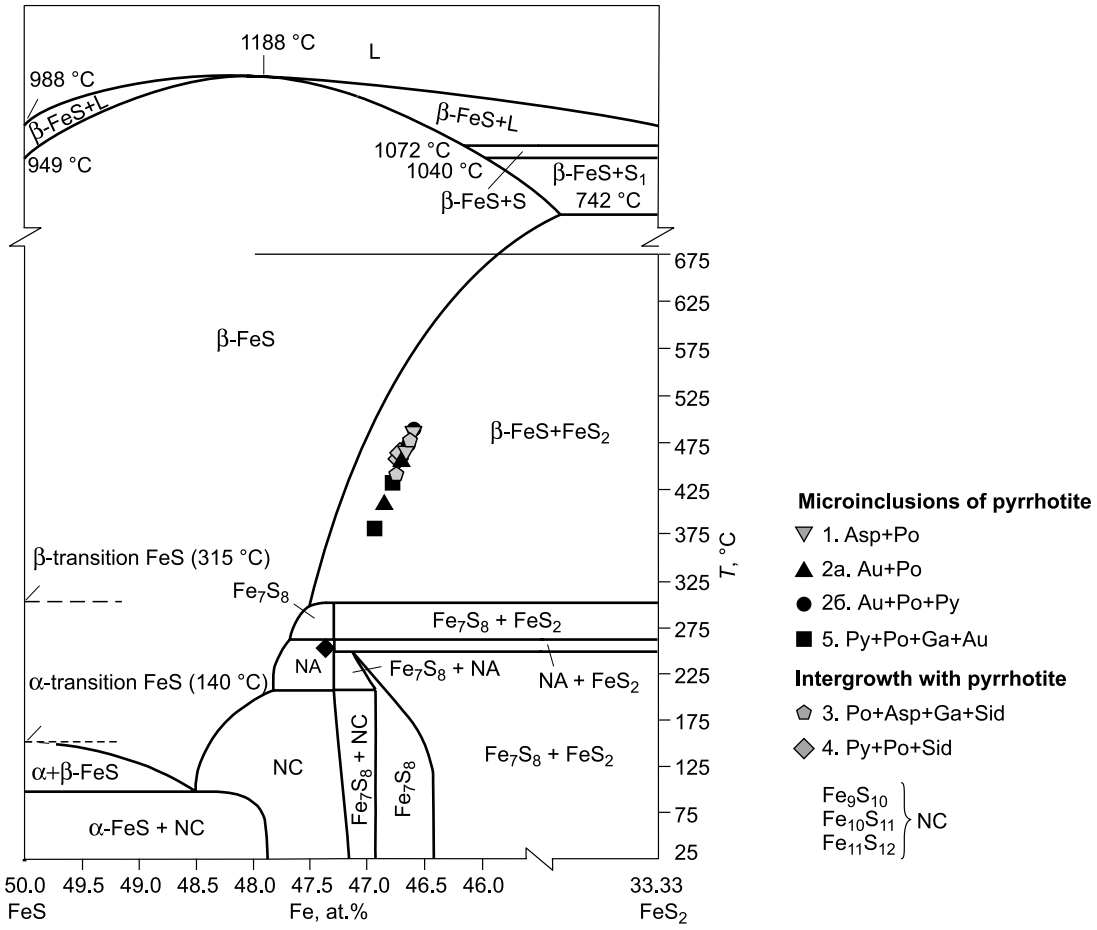

Fig. 10. Sulfur fugacity dependence on temperature for FeS–FeS_2 (Wang and Salveson, 2005), and log f_{S_2} estimations for different mineral associations with the pyrrhotite of different compositions and structures and/or pyrite that are typical for the Sovetskoe deposit. The associations are given in the order of their formation: 1, Asp + Po; 2, *a*, *b*, $Au_{(950)}$ + Po + Py; 3, Po + Asp + Ga + Sid; 4, Py + Po + Sid; 5, Py + Po + Ga + Au.

In (Barton, 1980; Gurevich et al., 2011) the authors present a log f_{S_2}–*T* diagram for system Ag–Au–S and a narrow temperature interval of 50–350 °C. Having extrapolated the thermodynamic constants for uytenbogaardtite, petrovskaite and Au_2S from (Osadchii and Rappo, 2004; Tagirov et al., 2006) we have extended the interval to 700 °C.

According to the experimental data (Barton, 1980) in Ag–Au–S three types of solid sulfide solutions exist at the temperatures of 300–700 °C. There are $Ag_{2-x}S$ ($x\rightarrow0$)–$Au_{0.1}Ag_{1.9}S$, $Au_{0.1}Ag_{1.9}S$–$Au_{0.4}Ag_{1.6}S$ и $Au_{0.4}Ag_{1.6}S$–$Au_{1.8}Ag_{0.2}S$ with face-centered (*F*), volume-centered (*I*) and primitive (*P*) cubic cells, respectively. As the temperature decreases, the $Ag_{2-x}Au_xS$ solid solutions transform into argentite/acanthite (β, α-Ag_2S), uytenbogaardtite (β, α-Ag_3AuS_2) and petrovskaite (β, α-AgAuS). To simplify the calculations, we used the solid solutions including extreme Ag_2S composition and intermediate $Ag_{1.5}Au_{0.5}S$ and $Ag_{1.0}Au_{1.0}S_2$ ones (identical to uytenbogaardtite and petrovskaite compositions), and Au_2S.

The other triplet (Fe–Ag–S) in the temperature interval of 320–600 °C produces three coexisting stable phases such as argentite, pyrrhotite and pyrite, but when the temperature decreases below 245 °C, it produces silver–pyrite associations developing due to coexistence of pyrrhotite and argentite (acanthite) (Taylor, 1970; Osadchii and Chareev, 2006). Such ternary compounds as sternbergite, argentopyrite, frieseite ($Ag_2Fe_5S_8$) and argiropyrite ($Ag_3Fe_7S_{11}$) are rare and can retain their stability even at lower temperatures. Fe–Au–S systems are also known to contain such gold sulfides as Au_2S, AuS, Au_2S_3, but they have never been found in nature, and their thermodynamic data have been established only for Au_2S. Thus, for some of the listed phases, it has been difficult to establish their stability fields due to the absence of thermodynamic functions.

The values of G_T phases in Fe–Ag–Au–S system used in the calculations can be found in Table 3. The chemical reaction equations for Ag–Au–S and Fe–S as well as the equilibrium constants and formulas to calculate sulfur fugacity at the temperatures of 25–700 °C are given in Tables 4 and 5.

In Ag–Au–S, sulfidation of Au–Ag alloys can occur in different ways (Gurevich et al., 2011; Palyanova et al., 2014):

Table 2. Au and Ag concentrations and Au/Ag ratios in pyrite and pyrrhotite from the Sovetskoe deposit

Sample No.	Lab No.	Mineral	Au, ppm	Ag, ppm	Au/Ag
Atomic absorption analysis					
1	103-1	Po	0.049	0.77	0.064
2	104	Po	0.025	0.46	0.054
3	106	Po	0.014	0.72	0.019
4	376	Po	2.460	1.03	2.388
5	427	Po	0.002	1.26	0.002
6	464	Po	0.003	1.43	0.002
7	467	Po	0.022	0.04	0.550
8	597	Po	0.003	1.80	0.002
9	665	Po	0.077	0.28	0.275
10	720	Po	0.004	0.53	0.008
11	3010	Po	0.019	0.72	0.026
12	3030	Po	0.019	1.06	0.018
13	3044	Po	0.026	2.26	0.012
14	3045	Po	0.013	2.00	0.007
15	117	Py	1.810	5.95	0.304
16	378	Py	5.580	1.14	4.895
17	413	Py	37.200	13.73	2.709
18	419	Py	1.210	1.26	0.960
19	467	Py	0.190	0.11	1.727
20	467	Py	0.050	0.83	0.060
21	497	Py	6.150	2.86	2.150
22	533	Py	0.180	0.17	1.059
23	598	Py	0.790	0.57	1.386
24	599	Py	0.093	0.34	0.274
25	616	Py	0.510	0.57	0.895
26	624	Py	7.280	7.44	0.978
27	629	Py	12.800	4.58	2.795
28	637	Py	1.020	5.15	0.198
29	657	Py	8.180	3.43	2.385
30	664	Py	16.680	56.62	0.295
ICP-MS					
31	2-22	Po	0.402	3.76	0.107
32	2-20	Po	6.102	4.88	1.250
33	1-1/3	Py	0.264	66.29	0.004
34	2-27	Py	0.150	0.43	0.345
35	2-27 (1)	Py	1.870	0.14	13.023
36	2-22	Py	1.471	0.51	2.857
37	2-20	Py	0.224	2.81	0.080
LA-ICP-MS					
38	23	Po-5	0.020	0.06	0.333
39	23	Po-5	bdl	0.410	—
40	2-1-28	Py-2	0.110	bdl	—
41	2-1-28	Py-2	0.4	bdl	—
42	ASP	Py_{Au}-2	2.780	0.690	4.029
43	ASP	Py_{Au}-2	2.600	0.270	9.630
44	ASP	Py_{Au}-2	7.640	0.560	13.643
45	23	Py-5	bdl	0.130	—

Note. Bdl, below detection limit.

$$4Ag_{1-x}Au_x + S_{2(g)} = 2(1 - 4x)Ag_2S + 4xAg_3AuS_2, \quad 0 < x_{Au} < 0.25, \tag{7}$$

$$4Ag_{1-x}Au_x + S_{2(g)} = 2(1 - 2x)Ag_3AuS_2 + 2(4x - 1)AgAuS, \quad 0.25 < x_{Au} < 0.5, \tag{8}$$

$$4Ag_{1-x}Au_x + S_{2(g)} = 4(1 - x)AgAuS + 2(2x - 1)Au_2S, \quad 0.5 < x_{Au} < 1. \tag{9}$$

Formation of this or that pair of gold and silver sulfides depends on the alloys' compositions that form within certain intervals, and the reaction constants (7)–(9) determined by the temperature and sulfur fugacity. Reactions 7–9 for the extreme compositions of Au–Ag alloy intervals at $x_{Au} = 0$; 0.25; 0.5 and 1 can be written in a simplified form that accounts for the formation of a single gold and/or silver sulfide (Table 4). The obtained calculation results can be seen in the $\lg f_{S_2}$–T diagram presented in Fig. 11.

The Fe–S system experienced desulfidation reactions (Table 5, Fig. 10) with formation of metallic iron, FeS troilite, Fe_7S_8 pyrrhotite, a $Fe_{1-x}S$ solid solution or other iron sulfides (Fe_9S_{10}, $Fe_{10}S_{11}$ or $Fe_{11}S_{12}$) that are stable even at temperatures below 320 °C. The temperature dependences of sulfur fugacity for sulfidation reactions of Au–Ag alloys (Table 4) and iron sulfide desulfidation (Table 5) are brought together in Fig. 11.

In the system Fe–S–Ag–Au, both types of reactions (iron sulfide desulfidation and sulfidation reactions of Au–Ag alloys) occurred simultaneously, and the intersection points for temperature dependences of sulfur fugacity and the reactions they compose corresponded to the temperature fixed points. The equilibrium quaternary association of Ag, Ag_2S, FeS_2 and Fe_7S_8 (Table 4 and 5) turned out to be stable at 245 °C and $\log f_{S_2} = -15$. These mineral parageneses serve as geothermometers: below 245 °C and at lower sulfur fugacity it is silver-pyrite paragenesis that turns out to be stable, while above 245 °C and at higher sulfur fugacity it is pyrrhotite—argentite one.

The equilibrium line of pyrite and monoclinic pyrrhotite (Fe_7S_8) intersected the equilibrium line of $Au_{0.25}Ag_{0.75}$ alloy (fineness 380‰) and of solid solution phase, whose composition is close to the one of uytenbogaardtite (Ag_3AuS_2) at the temperature of ~450 °C and $\log f_{S_2} = -4.8$. The intersections of pyrite and monoclinic pyrrhotite equilibrium lines, and the equilibrium lines of $Au_{0.5}Ag_{0.5}$ (fineness 650‰) and solid solution phase, whose composition is close to one of petrovskaite (AuAgS) occurred even at higher temperature and sulfur fugacity (~550 °C and $\log f_{S_2} = -1.6$).

The $\log f_{S_2}$–T diagram in Fig. 11 demonstrates that at the temperatures above 245 °C there are solid Au–Ag sulfide solutions $(Ag, Au)_2S$ in the domain of stable sulfur-rich pyrrhotite and pyrite. In this case, the pyrrhotite composition changed from 48.5 to 45.5 at.% Fe, and the composition of Au–Ag sulfides depended on both temperature and sulfur

Table 3. Gibbs free energies (GT, kcal/mol) of Fe–Ag–Au–S phases at the temperatures of 25–700 °C, used in calculations

Substance	Temperature, °C								Reference
	25	100	200	300	400	500	600	700	
$S_{2\,(g)}$	18.953	14.794	9.059	3.147	–2.915	–9.106	–15.409	–21.813	(Johnson et al., 1992)
$S^0_{(s,l)}$	0	–0.619	–1.593	–2.732	–4.015	–5.429	–6.963	–8.609	(Shock et al., 1997)
$Ag^0_{(s)}$	0	–0.816	–2.046	–3.407	–4.881	–6.452	–8.11	–9.848	(Helgeson et al., 1978)
$Ag_{0.75}Au_{0.25}$	–1.172	–2.184	–3.943	–6.069	–8.497	–11.187	–14.111	–17.253	(Palyanova, 2008)
$Ag_{0.5}Au_{0.5}$	–1.42	–2.331	–3.639	–5.065	–6.621	–8.318	–10.167	–12.18	(Palyanova, 2008)
$Ag_{0.25}Au_{0.75}$	–1.036	–1.815	–2.608	–3.255	–3.848	–4.454	–5.123	–5.899	(Palyanova, 2008)
$Au^0_{(s)}$	0	–0.939	–2.423	–4.120	–5.993	–8.016	–10.168	–12.436	(Robie and Hemingway, 1995)
$Fe^0_{(s)}$	0	–0.536	–1.391	–2.379	–3.483	–4.691	–5.994	–7.385	(Holland and Powell, 1990)
Ag_2S	–9.426	–12.160	–16.247	–20.752	–25.606	–30.756	–36.166	–41.804	(Knacke et al., 1991)
AgAuS	–6.592	–9.039	–12.702	–16.734	(–21.069)	(–25.662)	(–30.479)	(–35.459)	(Tagirov et al., 2006)
Ag_3AuS_2	–16.585	–21.804	–29.611	(–38.195)	(–47.421)	(–57.191)	(–67.436)	(–78.101)	(Tagirov et al., 2006)
FeS_2	–38.139	–39.221	–41.038	–43.218	–45.707	–48.467	–51.466	–54.681	(Waldner and Pelton, 2005)
FeS	–23.731	–25.079	–27.243	–30.025	–33.663	–38.367	–44.306	–51.620	(Waldner and Pelton, 2005)
Fe_7S_8	–215.196	–224.207	–237.000	–250.511	–	–	–	–	(Waldner and Pelton, 2005)
$Fe_{11}S_{12}$	–328.212	–342.199	–362.040	–382.980	–	–	–	–	(Waldner and Pelton, 2005)
$Fe_{10}S_{11}$	–299.974	–312.808	–331.007	350.210	–	–	–	–	(Waldner and Pelton, 2005)
Fe_9S_{10}	–271.659	–283.192	–299.510	–	–	–	–	–	(Waldner and Pelton, 2005)

Note. The data in brackets are thermodynamic data extrapolations.

Table 4. Reaction equations, equilibrium constants and sulfur fugacity at the temperatures of 25–700 ºC in Ag–Au–S system

Equilibrium phases	Reaction equations	log K at different *T*, °C								log f_{S_2}
		25	100	200	300	400	500	600	700	
$Ag^0_{(s)}$, $Au^0_{(s)}$, $S^0_{(s,l)}$, Ag_2S, Ag_3AuS_2, AgAuS										
$S^0_{(s,l)}$ / $S_{2\,(g)}$	$2S^0_{(s,l)} = S_{2(g)}$	–13.897	–9.392	–5.657	–3.284	–1.661	–0.495	0.371	1.032	log K_1
$Ag^0_{(s)}$ / Ag_2S	$4Ag^0_{(s)} + S_{2(g)} = 2Ag_2S$	27.721	21.002	15.415	11.830	9.342	7.519	6.128	5.031	–log K_2
$Ag_{0.75}Au_{0.25}$/Ag_3AuS_2	$4Ag_{0.75}Au_{0.25} + S_{2(g)} = Ag_3AuS_2$	22.621	16.322	10.578	(6.508)	(3.415)	(0.943)	(–1.105)	(–2.857)	–log K_3
$Ag_{0.5}Au_{0.5}$/AgAuS	$2Ag_{0.5}Au_{0.5} + 0.5S_{2(g)} = AgAuS$	9.700	6.897	4.598	3.118	(2.068)	(1.264)	(0.611)	(0.043)	–2log K_4

Note. The data in brackets are thermodynamic data extrapolations.

Table 5. Reaction equations, equilibrium constants and sulfur fugacity at the temperatures of 25–700 °C in Fe–S system

Equilibrium solid phase	Reaction equations	log K at different *T*, °C								lg f_{S_2}
		25	100	200	300	400	500	600	700	
FeS / $Fe^0_{(s)}$	$2FeS = 2Fe^0_{(s)} + S_{2(g)}$	–48.700	–37.422	–28.070	–22.285	–18.651	–16.465	–15.322	–14.969	log K
FeS_2 / FeS	$2FeS_2 = 2FeS + S_{2(g)}$				–11.262	–6.874	–3.136	–0.272	3.524	log K
FeS_2 /Fe_7S_8	$7FeS_2 = Fe_7S_8 + 3S_{2(g)}$	*–103.073*	*–73.867*	*–49.155*	*–32.870*	—	—	—	—	*⅓log K*
Fe_7S_8 / Fe_9S_{10}	$9Fe_7S_8 = 7Fe_9S_{10} + S_{2(g)}$	*–36.070*	*–26.760*	*–20.066*	—	—	—	—	—	*log K*
Fe_9S_{10} / $Fe_{10}S_{11}$	$10Fe_9S_{10} = 9Fe_{10}S_{11} + 0.5S_{2(g)}$	*–38.570*	*–28.172*	*–19.002*	—	—	—	—	—	*2log K*
$Fe_{10}S_{11}$ / $Fe_{11}S_{12}$	$11Fe_{10}S_{11} = 10Fe_{11}S_{12} + 0.5S_{2(g)}$	*–39.699*	*–30.808*	*–23.289*	*–18.368*	—	—	—	—	*2log K*
$Fe_{11}S_{12}$ / FeS	$Fe_{11}S_{12} = 11FeS + 0.5S_{2(g)}$	*–42.892*	*–35.716*	*–22.465*	*–13.197*	—	—	—	—	*2log K*

Note. The values of reaction constants marked in *italic* were calculated using the thermodynamic data from (Waldner and Pelton, 2005) and are shown in Fig. 11 in the low-temperature domain. In the high-temperature domain (>300 °C), the pyrrhotite composition is presented as a function of temperature and sulfur fugacity based on the equation from (Toulmin and Barton, 1964).

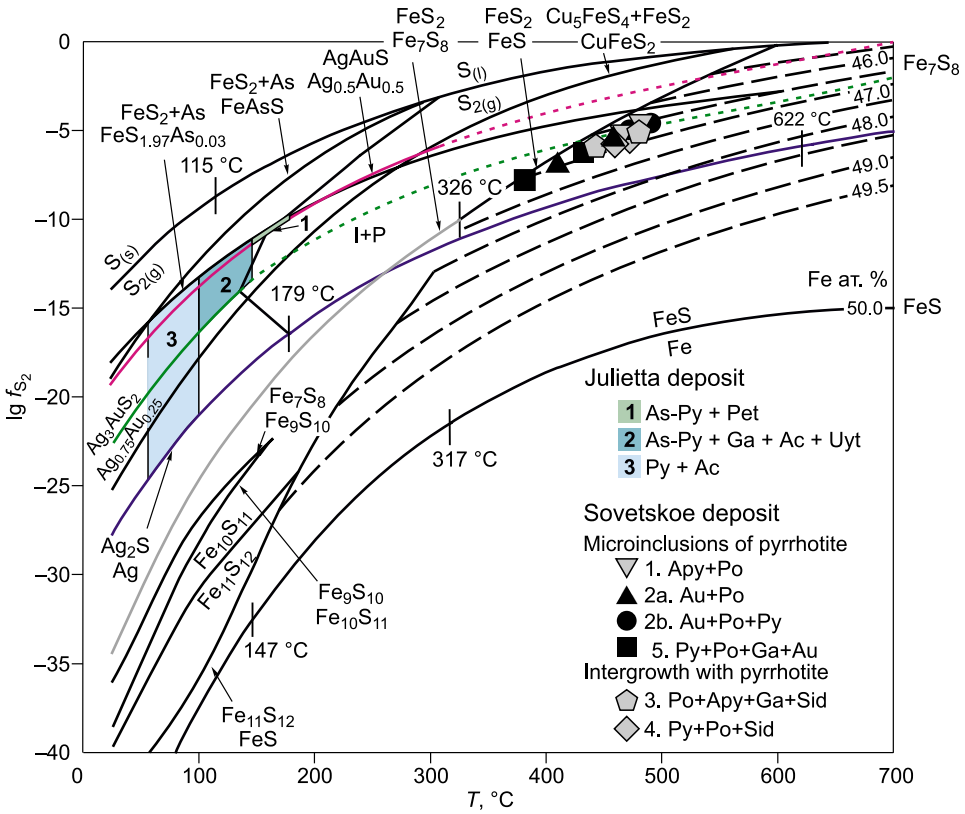

Fig. 11. Sulfur fugacity dependence on temperature for Fe–Au–Ag–S, and log f_{S_2} and T estimations for different associations with pyrrhotite from the Sovetskoe deposit.

fugacity: the higher the temperature the higher is the gold concentration in both the solid Au–Ag sulfide solution and Au–Ag alloy. For the high-temperature pyrite–pyrrhotite association with high sulfur content it is petrovskaite. As the temperature decreases and the amount of iron in pyrrhotite increases, it is uytenbogaardtite and/or acanthite.

At the temperatures below 245 °C the lowest sulfur fugacity values were typical for native silver paragenesis with FeS (troilite). As the sulfur fugacity increased, this paragenesis was followed by those of native silver with iron sulfides $Fe_{11}S_{12}$, $Fe_{10}S_{11}$ and Fe_9S_{10} and monoclinic pyrrhotite Fe_7S_8. Above the Ag–Ag_2S equilibrium line the stable pyrite paragenesis with native silver was replaced by a pyrite paragenesis with acanthite (argentite) and/or low fineness gold as the sulfur fugacity increased. The pyrite associated with uytenbogaardtite or a finer alloy ($Au_{0.25–0.5}Ag_{0.75–0.05}$, fineness 380–650‰) was stable even at higher values of sulfur fugacity. When the fugacity reaches its maximum value, it may provoke crystallization of pyrite with an alloy of fineness higher than 650‰ ($Au_{0.5}Ag_{0.5}$) and/or with petrovskaite.

According to the diagram in Fig. 11, the stability field of pyrite and sulfur-rich pyrrhotites in the Sovetskoe deposit lies in the stability field of solid Au–Ag sulfide solutions. The obtained results demonstrate that both pyrrhotites and pyrite of the deposit may contain solid Au–Ag sulfide solutions.

DISCUSSION

The pyrite-pyrrhotite paragenesis is present in many gold-ore deposits (Boyle, 1968; Petrovskaya et al., 1976; Boyle, 1979; Morrison et al., 1991; Large et al., 2011; Sazonov et al., 2014; Liang and Hoshino, 2015; Steadman and Large, 2016; etc.). The ores of many gold-sulfide deposits are regarded as refractory (Volkov and Sidorov, 2017). Deposits of impregnated sulfide refractory ores are a main potential source of gold in many countries due to their rich reserves. In such ores, gold presents either as inclusions in minerals or as invisible gold associated with iron sulfides. What is the occurrence type for noble metals in pyrite and pyrrhotite? In the case of invisible gold it is usually colloid, cluster, chemically-bonded gold (isomorphic and structural) or ultrafine gold that cannot be optically detected.

It is conventional knowledge that silver and gold occur in sulfide ores as native metals. According to the results obtained in the presented study, together with the native form of noble metals, a sulfide form can also turn out as stable in ores with pyrites and sulfur-rich pyrrhotite $Fe_{1-x}S$ ($0 \le x \le 0.125$) or FeS_y ($1 \le y \le 1.143$) (Fig. 11). In our opinion, the overlooked forms of silver and gold in iron sulfides can be ultrafine micron inclusions of gold and silver sulfides such as acanthite (α,β,γ-Ag_2S), uytenbogaardtite (α,β-Ag_3AuS_2), petrovskaite (α,β-AgAuS), and solid solutions $Ag_{2-x}Au_xS$ and

Au_2S. In (Ishikawa, 1995) the author proves the existence of Au_2S within the temperature range up to 147 °C (420 K).

Gold and silver sulfides are difficult to detect for a number of different reasons. First, they are characterized by low hardness (2–3), increased porosity, bad grindability and sufficient spall during sample preparation, which makes them similar to some other ore minerals such as sphalerite and fahlores. At the size of these microinclusions of 1–5 μm, their EPMA detection becomes impossible since it is prevented by the size of the background matrix containing iron and sulfur. In addition, silver-rich Au–Ag sulfides are unstable and are often destructed by an electron beam (Pal'yanova et al., 2014). In the recent years, these minerals have often been found in gold-sulfide ores (Majzlan, 2009; Pal'yanova and Savva, 2009; Savva et al., 2012; Palyanova et al., 2014; Cocker et al., 2013; Vikent'ev, 2015).

The results of our thermodynamic calculations have demonstrated that pyrrhotite Fe_7S_8 (member of solid pyrrhotite solutions that have the richest sulfur concentration, $x = 0.125$) and pyrite remain stable together with uytenbogaardtite and petrovskaite solid solutions (fineness more than 670‰, $Ag_{0.5}Au_{0.5}$–Au) at high temperature and sulfur fugacity values. Pyrrhotites with higher iron content (from $Fe_{0.875}S$ to FeS, $0 < x < 0.125$), pyrites, uytenbogaardtite and acanthite solid solutions, and electrum remain stable at moderate temperature and sulfur fugacity values.

Our thermodynamic calculations indicate that the formation of pyrrhotite-(pyrite)-bearing mineral associations in the Sovetskoe deposit occurred together with temperature decrease from 489 to 382 °C and log f_{S_2} from –4.63 to –7.95. These data correspond to the deposit genesis conditions determined by A.A. Tomilenko and N.A. Gibsher (2001) when studying fluid inclusions in the deposit vein quartz. The obtained deposition temperatures of pyrite-bearing associations are only insignificantly higher than the formation temperatures of the deposit quartz vein zones (100–410 °C) and match the interval of quartz ore vein formation (100–630 °C).

Figure 11 shows the stability fields of pyrite mineral associations with Au–Ag sulfides (petrovskaite, uytenbogaardtite and acanthite) in accord with their low-temperature formation conditions in the Julietta deposit of the Magadan region (Palyanova et al., 2016). If compared to this deposit, where a few pyrite generations have been indicated that contain petrovskaite, uytenbogaardtite and also acanthite rims—in the Sovetskoe deposit, pyrite, pyrrhotite, high fineness gold as well as the solid solutions of Au–Ag sulfides are formed at much higher temperature and sulfur fugacity values. So the obtained results are an indication that the ores of the Sovetskoe deposit probably contain petrovskaite and uytenbogaardtite in iron sulfides.

An additional proof of Au-Ag sulfides presence can be the value of Au/Ag mass ratios in pyrite-(pyrrhotite)-bearing ores. For many gold-sulfide deposits, native gold is a main or a dominating mineral of gold and silver. This is so if the Au/Ag mass ratio in ores is either equal or close to the Au/Ag ratio in native gold. This ratio in high fineness gold (950–990‰) varies from 19 to100; in native gold (fineness 500‰)—Au/Ag = 1; in native silver (fineness 100 and 1‰)—Au/Ag = 0.1÷0.001. But, if Au/Ag in ores is less than it is in native gold or silver, this is a sign the ore contains other silver minerals such as acanthite, petrovskaite, uytenbogaardtite, Ag sulfosalts, Au–Ag selenides (fischesserite, naumannite) and tellurides (hessite, stützite, petzite) (Pal'yanova, 2008; Palyanova, 2008; Liang and Hoshino, 2015).

In presence of invisible gold, the Au/Ag mass ratio in sulfide ores <20 is evidence of the particles, in which silver prevails over gold. These can be both sulfide and native forms of noble metals. For example, in uytenbogaardtite, the Au/Ag mass ratio equals to 0.6, and in petrovskaite 1.8. The gold-sulfide deposits of impregnated ores are characterized by the high Au/Ag values of 10:1 and higher, and only in case Au/Ag is above 16.4 such as in the solid solutions of Au-Ag sulfides with a maximum content of gold $Au_{1.8}Ag_{0.2}S$, can we conclude their absence.

Table 2 contains the data on gold and silver concentrations in the pyrrhotites and pyrites of the Sovetskoe deposit that have been obtained using ICP-MS, LA-ICP-MS and atomic absorption analysis. The Au/Ag ratios in pyrrhotites calculated from these data vary from 2.4 to 0.002, and in pyrites from 13 to 0.004. The results of assay tests in technological samples of ores from the Sovetskoe deposit indicate noble metals present in the following quantities: Au 1.8 ppm, Ag 5.0 ppm, and Au/Ag ratio is equal to 0.36. The Au/Ag values in the pyrrhotites and pyrites of the studied low sulfide-gold-quartz ores is lower than this value in high fineness gold (950–980‰ (≤19–50)). LA-ICP-MS studies of these pyrrhotites and pyrites have indicated the absence of Te, Se, Sb and Bi microinclusions, which is in favor of the possible presence of ultrafine Au–Ag sulfides. When the ores lack significant amounts of such elements as selenium, tellurium, antimony, bismuth and other elements forming stable associations with silver, it indicates a highly likely presence of gold and silver sulfides. Earlier works (Petrovskaya, 1954) mentioned the presence of native silver and freibergite among the minerals of late ore-forming stages in the Sovetskoe deposit.

For most gold-sulfide deposits, the Au/Ag ratio in ores and iron sulfides rarely reach 20–100, and in most cases vary from 1 to 10 and even less (Palyanova, 2008; Liang and Hoshino, 2015; Steadman and Large, 2016). Our forecast for gold-sulfide deposits with low Au/Ag ratios is that the refractory sulfide ores may contain Au–Ag sulfides, where acanthite, uytenbogaardtite and/or petrovskaite can occur in the iron sulfides as of gold as of gold-sulfide, porphyry-copper and copper-nickel deposits.

CONCLUSIONS

According to EPMA analysis, the compositions of pyrrhotites in the mineral associations of the northwestern part

of the Sovetskoe deposit have iron concentrations varying from 46.6 to 46.94 at.%, and sulfur concentrations from 53.4 to 53.06 at.%, which is from $Fe_{0.873\pm0.02}S$ to $Fe_{0.885\pm0.02}S$ in formula units.

Formation of pyrrhotite-(pyrite)-bearing mineral associations in the deposit occurred synchronously with the decrease in temperature from 489 to 382 °C and of sulfur fugacity – from –4.63 to –7.95. The obtained data lie within the temperature interval of quartz vein formation (100–630 °C) determined earlier using thermobarogeochemical methods (Tomilenko and Gibsher, 2001).

According to the $\log f_{S_2}$–T diagram, in the Fe–Ag–Au–S system the stability field of solid Au–Ag sulfide solutions $Ag_{2-y}Au_yS$ ($0 < y < 1.8$) corresponds with the pyrrhotite domain characterized by increased sulfur content, which allows us to suggest the presence of monodisperse Au–Ag sulfides (petrovskaite, uytenbogaardtite or acanthite) in the sulfide ores of the Sovetskoe deposit.

Lower Au/Ag ratio values in the deposit's pyrites and pyrrhotites if compared to this value in the deposit's native gold in absence of other chalcogens, confirm the presence of ultrafine silver inclusions, most likely Au–Ag sulfides.

For the deposit's quartz-gold-sulfide ores as in other deposits and mineral occurrences, the presence of ultrafine invisible particles of Au–Ag sulfides in association with native gold can be predicted.

This work is supported by state assignments of IGM SB RAS and ICCT SB RAS financed by Ministry of Science and Higher Education of the Russian Federation.

REFERENCES

Arnold, R.G., 1962. Equilibrium relations between pyrrhotite and pyrite from 325 degrees to 743 degrees C. Econ. Geol. 57 (1), 72–90.

Arnold, R.G., 1967. Range in composition and structure of 82 natural terrestrial pyrrhotites. Can. Mineral. 9 (1), 31–50.

Ballhaus, C., Bockrath, C., Wohlgemuth-Ueberwasser, C., Laurenz, V., Berndt, J., 2006. Fractionation of the noble metals by physical processes. Contrib. Mineral. Petrol. 152 (6), 667–684.

Barton, M.D., 1980. The Ag–Au–S system. Econ. Geol. 75 (2), 303–316.

Barton Jr., P.B., Toulmin, P., 1964. The electrum-tarnish method for the determination of the fugacity of sulfur in laboratory sulfide systems. Geochim. Cosmochim. Acta 28 (5), 619–640.

Bortnikov, N.S., Razdolina, N.V., Prokof'ev, V.Yu., 1996. Origin of the Charmitan gold-quartz deposit (Uzbekistan). Geol. Ore Deposits 38 (3), 208–226.

Boyle, R.W., 1968. The geochemistry of silver and its deposits. Geol. Surv. Can. Bull. 160, 183–190.

Boyle, R.W., 1979. The Geochemistry of Gold and Its Deposits. Ottawa, Geol. Surv. Canada.

Chareev, D.A., Osadchii, E.G., 2005. Pyrrhotite-pyrite equilibria in the Ag–Fe–S system et 245 to 310 °C and standart pressure. Geochem. Miner. Petrol. Bulgar. Acad. Sci. 43, 41–46.

Chareev, D.A., Voronin, M.V., Osadchii, E.G., 2014. Thermodynamic study of monoclinic pyrrhotite in equilibrium with pyrite in the Ag–Fe–S system by solid-state electrochemical cell technique. Am. Mineral. 99 (10), 2031–2034.

Cocker, H.A., Mauk, J.L., Rabone, S.D.C., 2013. The origin of Ag–Au–S–Se minerals in adularia-sericite epithermal deposits: constraints from the Broken Hills deposit, Hauraki Goldfield, New Zealand. Miner. Deposita 48, 249–266.

Craig, J.R., Vokes, F.M., 1993. The metamorphism of pyrite and pyritic ores: an overview. Mineral. Mag. 57, 3–18.

Godovikov A.A., 1983. Mineralogy [in Russian]. Nedra, Moscow.

Gordon, S.C., McDonald, A.M., 2015. A study of the composition, distribution, and genesis of pyrrhotite in the copper cliff offset, Sudbury, Ontario. Can. Mineral. 53, 859–878.

Gronvold, F., Stolen, S., 1992. Thermodynamics of iron sulfides II. Heat capacity and thermodynamic properties of FeS and $Fe_{0.875}S$ at temperatures from 298.15 K to 1000 K, of $Fe_{0.98}S$ from 298.15 K to 800 K, and $Fe_{0.89}S$ from 298.15 K to about 650 K. Thermodynamics of formation. J. Chem. Thermodyn. 24 (9), 913–936.

Gurevich, V.M., Gavrichev, K.S., Osadchii, E.G., Tyurin, A.V., Ryumin, M.A. 2011. Heat capacity and thermodynamic functions of petrovskaite (AgAuS) at 0–583 K and mineral equilibria in the Ag–Au–S system. Geochem. Int. 49 (4), 442–448.

Helgeson, H.C., Delany, J.M., Nesbitt, H.W., Bird, D.K., 1978. Summary and critique of the thermodynamic properties of rock-forming minerals. Am. J. Sci. 278A, 1–229.

Holland, H.D., 1965. Some applications of thermochemical data to problems of ore deposits; [Part] 2, Mineral assemblages and the composition of ore forming fluids. Econ. Geol. 60 (6), 1101–1166.

Holland, T.J.B., Powell, R., 1990. An enlarged and updated internally consistent thermodynamic dataset with uncertainties and correlations: the system K_2O–Na_2O–CaO–MgO–FeO–Fe_2O_3–Al_2O_3–TiO_2–SiO_2–C–H_2–O_2. J. Metamorph. Geol. 8 (1), 89–124.

Ishikawa, K., Isonaga, T., Wakita, S., Suzuki, Y., 1995. Structure and electrical properties of Au_2S. Solid State Ionics 79, 60–66.

Johnson, J.W., Oelkers, E.H., Helgeson, H.C., 1992. SUPCRT92: software package for calculating the standard molal thermodynamic properties of mineral, gases, aqueous species, and reactions from 1 to 5000 bars and 0 to 1000 °C. Comput. Geosci. 18, 899–947.

Knacke, O., Kubaschewski, O., Hesselmann, K., 1991. Thermochemical Properties of Inorganic Substances. Springer-Verlag, Heidelberg.

Kolonin, G.R., Pal'yanova, G.A., 1991. Arsenopyrite-containing mineral associations as indicators of the physicochemical conditions of hydrothermal ore formation. Geokhimiya, No. 10, 1481–1492.

Kolonin, G.R., Gas'kova, O.L., Pal'yanova, G.A., 1986. Experience in identifying mineralization facies based on buffer parageneses of sulfide minerals. Geologiya i Geofizika (Soviet Geology and Geophysics) 27 (7), 133–141 (116–123).

Kretschmar, U., Scott, S.D., 1976. Phase relations involving arsenopyrite in the system Fe–As–S and their application. Can. Mineral. 14 (3), 364–386.

Lambert, J.M., Simkovich, J.R., Walker, P.L., 1998. The kinetics and mechanism of the pyrite-to-pyrrhotite transformation. Metall. Mater. Trans. B 29B, 385–396.

Large, R.R., Bull, S.W., Maslennikov, V.V., 2011. A carbonaceous sedimentary source-rock model for carlin-type and orogenic gold deposits. Econ. Geol. 106, 331–358.

Lennie, A.R., Vaughan, D.J., 1996. Spectroscopic studies of iron sulfide formation and phase relations at low temperatures. Miner. Spectrosc., Spec. Publ. 5, 117–131.

Liang, Y., Hoshino, K., 2015. Thermodynamic calculations of Aux Ag1-x—fluid equilibria and their applications for ore-forming conditions. Appl. Geochem. 52, 109–117.

Majzlan, J., 2009. Ore mineralization at the Rabenstein occurrence near Banska Hodrusa, Slovakia. Mineralia Slovaca 41, 45–54.

Moloshag, V.P., 2009. Using the composition of minerals to assess the physico-chemical conditions for the formation of pyritic ores of the Urals. Litosfera, No. 2, 28–40.

Morrison, G.W., Rose, W.J., Jareith, S., 1991. Geological and geochemical controls on the silver content (fineness) of gold in gold-silver deposits. Ore Geol. Rev. 6, 333–364.

Osadchii, E.G., Chareev, D.A., 2006. Thermodynamic studies of pyrrhotite–pyrite equilibria in the Ag–Fe–S system by solid-state galvanic cell technique at 518–723 K and total pressure of 1 atm. Geochim. Cosmochim. Acta 70, 5617–5633.

Osadchii, E.G., Rappo, O.A., 2004. Determination of standard thermodynamic properties of sulfides in the Ag–Au–S system by means of a solid-state galvanic cell. Am. Mineral. 89 (10), 1405–1410.

Pal'yanova, G., 2008. Physicochemical modeling of the coupled behavior of gold and silver in hydrothermal processes: gold fineness, Au/Ag ratios and their possible implications. Chem. Geol. 255 (3–4), 399–413.

Pal'yanova, G.A., Savva, N.E., 2009. Specific genesis of gold and silver sulfides at the Yunoe deposit (Magadan Region, Russia). Russian Geology and Geophysics (Geologiya i Geofizika) 50 (7), 587–602 (759–777).

Palyanova, G., Karmanov, N., Savva, N., 2014. Sulfidation of native gold. Am. Mineral. 99 (5–6), 1095–1103.

Palyanova, G.A., 2008. Physical and Chemical Peculiarities of Silver and Gold Behavior while Geothermal Ore Genesis [in Russian]. ISO RAN, Novosibirsk.

Palyanova, G.A., Savva, N.E., Zhuravkova, T.V., Kolova, E.E., 2016. Gold and silver minerals in low-sulfidaton ores of the Julietta deposit (northeastern Russia). Russian Geology and Geophysics (Geologiya i Geofizika) 57 (8), 1171–1190 (1486–1508).

Paton, C., Hellstrom, J., Paul, B., Woodhead, J., Hergt, J., 2011. Iolite: Freeware for the visualisation and processing of mass spectrometric data. J. Anal. Atom. Spectrosc. 26, 2508–2518.

Petrovskaya, N.V., 1954. Gold Mineralization of the Yenisei Ridge and Gold Ore-Forming Processes. ScD Thesis [in Russian]. NIGRIZOLOTO, Moscow.

Petrovskaya, N.V., Safonov, Yu.G., Sher, S.D., 1976. Gold ore genesis, in: Ore Formations of Endogenic Deposits. Vol. 2: Formation of Endogenic Gold, Gold-Sulfide, Lead, Zinc and Mercury Deposits [in Russian]. Nauka, Moscow, pp. 3–110.

Robie, R.A., Hemingway, B.S., 1995. Thermodynamic properties of minerals and related substancies of 298.15 K and 1 bar pressure and at higher temperatures. U.S. Geol. Surv. Bull. 2113. DOI: 10.3133/b2131.

Rottier, B., Kouzmanov, K., Wälle, M., Bendezú, R., Fontboté, L., 2016. Sulfide Replacement Processes Revealed by Textural and LA-ICP-MS Trace Element Analyses: Example from the Early Mineralization Stages at Cerro de Pasco, Peru. Econ. Geol. 111, 1347–1367.

Rusinova, O.V., Rusinov, V.L., Abramov, S.S., Kuznetsova, S.V., Vasyuta, Yu.V., 1999. Wallrock alterations and physical-chemical formation conditions of the Sovetskoe gold-quartz deposit (Yenisei Ridge, Russia). Geologiya Rudnykh Mestorozhdenii 41 (4), 308–328.

Sack, R.O., Ebel, D.S., 2006. Thermochemistry of Sulfide Mineral Solutions. Rev. Mineral. Geochem. 61, 265–364.

Savva, N.E., Pal'yanova, G.A., Byankin, M.A., 2012. The problem of genesis of gold and silver sulfides and selenides in the Kupol deposit (Chukotka, Russia). Russian Geology and Geophysics (Geologiya i Geofizika) 53 (5), 457–466 (597–609).

Sazonov, A.M., Saraev, V.A., Ananyev, A.A., 1991. Sulfide-quartz deposits of gold in metamorphic series of the Yenisei ridge. Geologiya i Geofizika (Soviet Geology and Geophysics) 32, 28–36 (23–32).

Sazonov, A.M., Zvyagina, E.A., Krivoputskaya, L.M., Sverdlova, V.G., Leontiev, S.I., 1992. Structural and chemical heterogeneities of the pyrite from the Saralinskoe deposit (Kuznetsk Alatau). Geologiya i Geofizika (Russian Geology and Geophysics) 33, 87–95 (77–84).

Sazonov, A.M., Onyfrienok, V.V., Kolmakov, Yu.V., Nekrasova, N.A., 2014. Gold ore pyrrhotite: composition, point defects, magnetic properties, gold distribution. Zhurnal Sibirskogo Federal'nogo Universiteta. Ser. Tekhnika i Tekhnologiya 6 (7), 717–737.

Scott, S.D., 1976. Application of the sphalerite geobarometer to regionally metamorphosed terrains. Am. Mineral. 61, 661–670.

Shi, P., 1992. Fluid fugacities and phase equilibria in the Fe–Si–O–H–S system. Am. Mineral. 77, 1050–1066.

Shock, E.L., Sassani, D.C., Willis, M., Sverjensky, D.A., 1997. Inorganic species in geologic fluids: Correlations among standard molal thermodynamic properties of aqueous ions and hydroxide complexes. Geochim. Cosmochim. Acta 61 (5), 907–950.

Silyanov, S.A., Nekrasova, N.A., 2015. Thermobaric geochemistry of vein quartz inclusions of the Sovetskoe gold deposit (Yenisei Ridge), in: Abstract Collection of the 5th Russian Youth Scientific and Practical School with International Participation "New about ore-forming" [in Russian]. IGEM RAN, Moscow.

Simon, G., Essene, E.J., 1996. Phase relations among selenides, sulfides, tellurides, and oxides. I, Thermodynamic properties and calculated equilibria. Econ. Geol. 91 (7), 1183–1208.

Skornyakov, P.I., 1947. Pyrrhotite pseudomorphs in pyrite. Kolyma, No. 2, 26–29.

Smirnov, V.I., 1978. Ore Deposits of the USSR (in 3 volumes) [in Russian]. Nedra, Moscow, Vol. 3.

Steadman, J.A., Large, R.R., 2016. Synsedimentary, diagenetic, and metamorphic pyrite, pyrrhotite, and marcasite at the Homestake BIF-hosted gold deposit, South Dakota, USA: Insights on Au–As ore genesis from textural and LA-ICP-MS trace element studies. Econ. Geol. 111 (7), 1731–1752.

Tagirov, B.R., Baranova, N.N., Zotov, A.V., Schott, J., Bannykh, L.N., 2006. Experimental determination of the stabilities of $Au_2S_{(cr)}$ at 25 °C and $Au(HS)_2^-$ at 25–250 °C. Geochim. Cosmochim. Acta, 70 (14), 3689–3701.

Taylor, L.A., 1970. The system Ag–Fe–S: Phase equilibria and mineral assemblages. Miner. Deposita 5, 41–58.

Tomilenko, A.A., Gibsher, N.A., 2001. Peculiarities of fluid composition in the mineralized and barren zones of the Sovetskoe quartz-gold deposit, Yenisei Mountain Range based on fluid inclusion study. Geochem. Int. 39 (2), 142–152.

Toulmin, P., Barton Jr., P.B., 1964. A thermodynamic study of pyrite and pyrrhotite. Geochim. Cosmochim. Acta 28, 641–671.

Tyukova, E.A., Voroshin, S.V., 2007. Composition and Parageneses of Arsenopyrite in Ores and Enveloping Rocks of the Upper Kolyma Region (about Interpretation of Sulfide Association Genesis) [in Russian]. SVKNII DVO RAN, Magadan.

Vikentyev, I.V., 2015. Invisible and microscopic gold in pyrite: Methods and new data for massive sulfide ores of the Urals. Geol. Ore Deposits 57 (4), 237–265.

Volkov, A.V., Sidorov, A.A., 2017. Invisible gold. Vestnik RAN 87 (1), 40–49.

Waldner P., Pelton, A.D., 2005. Thermodynamic modeling of the Fe–S system. J. Phase Equilib. Diffus. 26 (1), 23–38. (http://thermoddem.brgm.fr/data/espece.php?espece=m&i=227#fiche)

Wang, H., Salveson, I., 2005. A review on the mineral chemistry of the non-stoichiometric iron sulphide, $Fe_{1-x}S$ ($0 \le x \le 0.125$): polymorphs, phase relations and transitions, electronic and magnetic structures. Phase Transitions 78, 547–567.

Wang, H., Pring, A., Wu, F., Chen, G., Jiang, J., Xia, F., Zhang, J., Ngothai, Y., O'Neill, B., 2006. Effect of cation vacancy and crystal superstructure on thermodynamics of iron monosulfides. J. Sulfur Chem. 27 (3), 271–282.

Editorial responsibility: A.S. Borisenko